Science of the Total Environment 810 (2022) 151183

Contents lists available at ScienceDirect

Science of the Total Environment

journal homepage: www.elsevier.com/locate/scitotenv

Multiproxy characterization of sedimentary facies in a submarine sulphide mine tailings dumping site and their environmental significance: The study case of Portmán Bay (SE Spain)

Andrea Baza-Varas [a], Miquel Canals [a,*], Jaime Frigola [a], Marc Cerdà-Domènech [a], Nil Rodés [a], Marta Tarrés [a], Anna Sanchez-Vidal [a], and the NUREIEVA-MAR1 shipboard party [1]

[a] CRG Marine Geosciences, Department of Earth and Ocean Dynamics, Earth Sciences Faculty, University of Barcelona, Spain

HIGHLIGHTS

- A comprehensive assessment of a shallow water mine waste dumping site
- A multiproxy study of physicochemical properties of sedimentary facies
- Non-destructive, high-resolution, continuous sediment core analytical techniques
- Sediment properties unveil the environmental evolution of the dumping site.
- Ecosystem recovery back to natural conditions unlikely in studied dumping sites

GRAPHICAL ABSTRACT

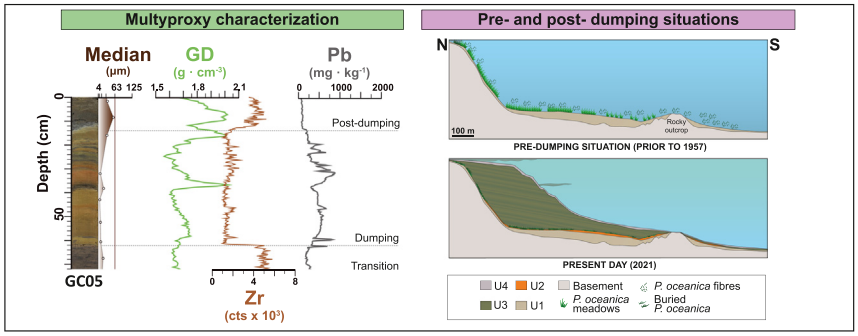

ARTICLE INFO

Article history:
Received 6 September 2021
Received in revised form 19 October 2021
Accepted 20 October 2021
Available online 29 October 2021

Editor: Damia Barcelo

Keywords:
Mine waste
Metal-rich deposit
Chemical-physical properties
Non-destructive sediment core analysis
Shallow coastal sea
Ecosystem impact

ABSTRACT

Mining activities are essential to our society, but ore extraction and treatment produce waste that must be stored in safe places without harm to the environment. For a long time, seafloor disposal has been viewed as a cheap option with barely visible impacts. In Portmán Bay, SE of Spain, large amounts of tailings from open pit sulphide mining were discharged directly into the coastal sea over 33 years, thus forming a massive deposit that completely infilled the bay and expanded seawards over the inner continental shelf. Here we present the first multiproxy physicochemical characterization of the submarine tailings in Portmán Bay, mostly by using non-destructive techniques, also including pre-dumping and post-dumping sediments. Eight distinct sedimentary facies, grouped in four stratigraphic units, have been thus identified in a set of up to 4.3 m long gravity cores totalling more than 60 m. Geogenic and anthropogenic geochemical proxies consistently allow differentiating pre-dumping sediments from tailings. Potentially toxic metals if made bioavailable can reach high concentrations in units including or formed exclusively by tailings (i.e. up to 3455, 2755 and 1007 mg kg^{-1} for Pb, As, and Zn, respectively). Some physical properties, such as magnetic susceptibility, are particularly useful as the tailings are rich in Fe-bearing minerals (>30% Fe in some layers). Estimated sedimentation rates show a strong gradient from proximal to distal locations, with rates in excess of 50 cm yr^{-1} to less than 1 cm yr^{-1}. We ultimately document the history of the transformation of Portmán Bay from an almost natural state to a new condition

* Corresponding author at: GRC Marine Geosciences, Department of Earth and Ocean Dynamics, Earth Sciences Faculty, Martí i Franquès, s/n, E-08028 Barcelona, Spain.
E-mail address: miquelcanals@ub.edu (M. Canals).
[1] D. Amblàs [a], X. Rayo [a], E. Soldevila [a], J. Rivera [b], G. Lastras [a], J. Roqué [c]
[b] Instituto Español de Oceanografía, Corazón de María 8, Madrid E-28002, Spain
[c] RG Mineral Resources, Department of Mineralogy, Petrology and Applied Geology, Earth Sciences Faculty, University of Barcelona, Barcelona E-08028, Spain

https://doi.org/10.1016/j.scitotenv.2021.151183

after a long period of massive dumping of mine tailings. Our study provides guidance to further assessments in a context where the diversity of marine environments impacted by the disposal of mine waste is expected to grow in the near future.

1. Introduction

Exploitation of mineral ores inevitably results in a variety of raw, processed and refusal materials that must be moved, stored, managed and eventually disposed according to legislations that differ from one place to another, and also through time. Refusal materials mostly include low-grade rock fragments and tailings, i.e. the waste material left over after the valuable component has been removed through processing (Roche et al., 2017). Fine-grained tailings usually consist of slurries with variable proportions of non-profitable ore, chemicals used during ore treatment, and water. Usually, tailings are disposed close to mining sites on land, most often in natural depressions or artificial landfills behind dams (Dold, 2014). Leakage to the ground or even collapse from such landfills is not unusual, as illustrated by the Aznalcóllar case, in Spain in 1998, amongst many others elsewhere (Mateos, 2001; Roche et al., 2017). Discharge of tailings to rivers (River Tailings Disposal, RTD) and to the sea (Submarine/Sea Tailings Disposal, STD) have been used as alternatives to land disposal, since capital and operating costs are usually low, as seen in Chile, France, Greece, Indonesia, Norway, Spain, Turkey, the United Kingdom and, mainly, Papua-New Guinea (Dold, 2014; Ramirez-Llodra et al., 2015).

Today, in many countries, mining companies have to minimize as much as possible the environmental impacts of their activities during exploration, exploitation and also after the cessation of exploitation. Pre-mining environmental impact assessments (EIAs), environmental monitoring during exploitation, and careful closure and restoration planning are now mandatory in most countries (Noble and Bronson, 2005; Monjezi et al., 2009; Oyarzun et al., 2011; Kabir et al., 2015; Morrison-Saunders et al., 2016; Vare et al., 2018). Since the 70's in the last century, global and regional conventions such as the London Convention of 1972 (IMO, 1972; Vogt, 2013) and the Barcelona Convention of 1995 (UNEP, 1995), together with European and national legislations (Dold, 2014; Walder, 2014), have established frames to reduce the environmental impacts derived from tailings storage on the seafloor. However, their implementation is uneven and some are in application since a rather short time, such as the London Convention, which is in force from 2006 only.

Besides legislation efforts, there are countless cases of environmental impacts because of submarine mine tailings disposal (Koski, 2012; Dold, 2014). For many of them, EIAs or impact monitoring have not been carried out ever. Actually, submarine disposal was legally permitted at the time. The environmental effects of sub-sea tailings accumulation depend on their composition, physical and chemical characteristics, volume and spatial extent, and also on the way tailings interact with the receiving environment (Walder, 2014).

Three main options appear recurrently in discussions about the recovery of seafloor areas covered by mining waste, which are: (1) the "leave as is and let the nature play" option (i.e. doing nothing), (2) the capping of the affected areas with more "natural" materials aiming at easing nature's come back option (i.e. a soft solution), and (3) the removal of waste option (i.e. a hard solution). For the third option, the main concern is whether or not the removal could cause further harm to the environment. Before eventually proceeding, wastes must be fully characterized so that their properties, behaviour and ecotoxicological potential are known in order to thereby ensure to the best possible extent that they could be managed under environmentally safe conditions in the short and long terms (European Commission Decision 2009/360/EC in OJEU, 2009). A subsequent need is the characterization of the extracted waste to ease a scientifically sound identification of realistic and feasible management options (e.g. secondary disposal, incineration, and reuse) altogether with related mitigation measures to protect human health and the environment. Such limitations and unknowns may explain the lack of actual cases of large-scale removal operations of seafloor mine tailings to date.

One of those places where major unknowns around potential removal concur is Portmán Bay, in La Unión mining district (Murcia, SE Spain). There, the original, scenic horseshoe-shaped bay was dramatically impacted by essentially unrestricted and unmonitored, though legally permitted, disposal of tailings from open pit Pb-Zn sulphide ore mining in the nearby Sierra Minera de Cartagena along 33 years, from 1957 to 1990 (Oen et al., 1975; Manteca and Ovejero, 1992). Ores went through a processing plant named "*Lavadero Roberto*", at a rate of ~1000 t d^{-1} in the first years that grew up to ~8000 t d^{-1} in the last years (Banos-González and Páez, 2013). Estimates indicate that about 60 Mt. of rock ores were processed resulting in 56.5 Mt. of waste (i.e. 25 Mm^3), most of which ended up into the sea (Martínez-Sánchez et al., 2015). Such a waste volume infilled most of the original bay, caused an up to ~600 m seaward shoreline shift, and completely sealed the natural seabed over a large area offshore. The later was still unacknowledged until very recently, despite its relevance amongst all changes in Portmán Bay and its surroundings due to mine tailings. Decades-long claims for a remediation plan for Portmán Bay led to the approval of a restoration project in 2011 to move back the shoreline by ~250 m by partially dredging the subaerial deposit (Decision of the 10th of February 2011 in BOE, 2011). However, this project barely started and is nowadays stopped because of lawsuits (Banos-González et al., 2017).

The behaviour and bioavailability of heavy metals, including transfers between sediment and water, and their ecotoxicological consequences, is one of the main concerns regarding the mine tailings deposit in Portmán Bay (Martínez-Sánchez et al., 2011; Duodu et al., 2017). Several studies on the marine extension of the Portmán Bay mine tailings deposits focused, therefore, on ecological and biological aspects. Not only the dumping led to the disappearance by burial and pollution of *Posidonia oceanica* — a Mediterranean endemism — seagrass meadows (Banos-González and Páez, 2013; Ruiz et al., 2015), but also some of the highest concentrations of Pb, As, Cd and Hg in marine organisms along the entire Spanish Mediterranean coast have been observed in the area long after waste disposal stopped (Benedicto et al., 2008). Other studies also focusing on biota-metals interactions are those from Auernheimer and Chinchon (1997) and Martínez-Gómez et al. (2012). More recent data from two fish species might indicate a lessening of Hg pollution in marine organisms, which would now be compliant with European legislation (Llull et al., 2017). In another rather recent study Mestre et al. (2017) characterized the in situ effects on mussels (*Mytilus galloprovincialis*) of artificially resuspended sediments atop of the tailings deposit by means of toxicity bioassays combined with sediment geochemical analyses, whereas Gambi et al. (2020) assessed the impact of sulphide mine tailings on meiofaunal assemblages.

Most studies looking specifically at the mine tailings deposit have focused on its emerged part that infills the older Portmán Bay. Such studies address the infill history (Oyarzun et al., 2013; Gómez-Garcia et al., 2015), the potential interest of the tailings as a secondary ore (Matínez-Sánchez et al., 2013; Manteca et al., 2014), the geochemical characterization of the materials (Martínez-Sánchez et al., 2008, 2011;

García-Lorenzo et al., 2012, 2014a), and the pollution of soils and groundwater (Robles-Arenas et al., 2006; García-García, 2004; García-Lorenzo et al., 2014a, 2014b). In contrast, only two recent studies deal with the submerged extension of the mine tailings deposit. The first of them addresses the remobilization of dissolved metals in the tailings by groundwater discharge and pore water exchange (Alorda-Kleinglass et al., 2019), while the second is method-oriented (Cerdà-Domènech et al., 2020).

Here we present an innovative and comprehensive multiproxy physicochemical assessment of the materials forming the submarine extension of a modern coastal sulphide mine tailings deposit and underlying materials, with the main objective of identifying its internal variability in terms of sedimentary facies and the properties that come with, and also as a tool to reconstruct in detail the deposit development and associated processes. This is an area where knowledge is lacking almost completely as, in practical terms, mine wasting deposits tend to be considered essentially homogeneous, which likely is a wrong assumption in a substantial number of cases at least. A secondary objective is bringing light to the transformations leading to the local extinction of *P. oceanica* meadows. To achieve our objectives we rely on a comprehensive analysis of several meters long sediment cores totalling more than 60 m in length. In contrast with Cerdà-Domènech et al. (2020), who only dealt with the uppermost centimetres of the submarine mine tailings deposit after a limited number of short multicores, we address in this paper the composition and properties of such anthropogenic deposit in a large number of cores down to several meters below the seafloor.

2. Study area

2.1. Overall setting

The study area is the inner continental shelf down to 55 m water depth off Portmán Bay (Fig. 1). The continental shelf there is 11 km wide, slopes less than 1° seaward and naturally is sediment-starved, as there are no relevant and permanent river mouths nearby (Acosta et al., 2013; Durán et al., 2018). In absence of human perturbations, such a lack of terrigenous supplies favours water transparency and eases the development of extensive seagrass meadows down to 40–45 m of water depth (Ruiz and Romero, 2001; Marbà et al., 2014; Ruiz et al., 2015). Seaward sediment transport is activated only during rare major storms, when almost permanently dry riverbeds, i.e. "ramblas" or wadis, carry water and sediment loads in the form of flash floods (Maldonado and Zamarreño, 1983).

A cross section normal to the isobaths shows a very shallow terrace at the innermost shelf down to 8–10 m depth that opens to a Gilbert delta type slope reaching 35–38 m at its foot, followed by a much smoother section extending to the southern end of the study area (Fig. 1). The bathymetry also depicts two parallel, NW–SE oriented straight ridges up to 4 m high crossing part of the study area, which have been previously interpreted as fault scarps (Acosta et al., 2013), though they may also correspond to beach rocks similar to those observed east of the nearby Mar Menor coastal lagoon (Fernández-Salas et al., 2015), or to a combination of the two.

Climate in the study area is typical arid to sub-arid Mediterranean, with hot summers (mean temperature, Tm = 24.2 °C) and mild winters (Tm = 11.4 °C), for an annual mean of 17.6 °C (data from the nearby San Javier airport meteorological station provided by *Agencia Estatal de Meteorología* (AEMET) for the period 1981–2010), and about 300 mm of annual rainfall (https://es.climate-data.org/europe/espana/region-de-murcia/cartagena-3213/). Such meagre precipitation occurs by means of few rainfall events in the hydrological year that directly and solely determine the recharge of the Sierra Minera de Cartagena aquifer (Robles-Arenas, 2007). Groundwater in the study area and in the broader Sierra Minera district displays a considerable level of metal pollution that makes those waters unusable for human consumption and often also for land irrigation purposes according to the Spanish (Royal Decree 140/2003 in BOE, 2003) and European (Council Directive 98/83/CE in OJEC, 1998) water quality guidelines, mainly due to excess sulphate and Mn concentrations, and elevated electric conductivity (García-García, 2004; Robles-Arenas et al., 2006). Sulphide mineral oxidation leading to the formation of new sulphide minerals and the dissolution of the later appear as the main geochemical processes that are responsible for, subsequently resulting in acid-mine drainage that eases metal mobility because of the associated decrease in pH (Robles-Arenas et al., 2006, and references therein). Submarine groundwater discharge constitutes the main source of dissolved Fe to the coastal sea, whereas porewater exchange drives the remobilization and supply of most dissolved metals (Alorda-Kleinglass et al., 2019).

In parallel with air temperatures, wind and sea waves also have different summer and winter regimes. In summer, wind blows mostly from the NE while wave direction is essentially from the east, with significant wave heights (Hs) of 1–2 m. In wintertime wind direction shifts form one direction to another, with SW and NE appearing as the prevailing directions, with 2–3 m of Hs waves coming mostly from the SW and ENE (data from SIMAR maritime simulation system of *Puertos del Estado* for point 20,774,090 located at 37°30′N and 0°49.48′W). Currents in the study area are dominated by wind and wave action (Pauc and Thibault, 1976), and are mostly influenced by the southernmost extension of the Northern Current, a coastline-parallel mesoscale current originated in the Northwestern Mediterranean region or by eastwards and northwards surface Atlantic Water coming from the Strait of Gibraltar and the Alboran Sea (Millot and Taupier-Letage, 2005).

2.2. Mining history and waste composition

Long before the last period of open pit ore exploitation (cf. Section 1), mining in Sierra Minera de Cartagena was already practiced in prehistoric times, with Pb, Zn, Ag, Fe, Cu, Sn, Mn, and barite in hydrothermal sulphides as main targets (Manteca and Ovejero, 1992; Manteca et al., 2014; Sabaté et al., 2015). Small-scale underground mining kept on, though with some periods of abandonment, over an area of about 50 km^2 (García-García, 2004) until mid-20th century when the large-scale open pit activities started, subsequently resulting in a tremendous impact over the Sierra's landscape and in large amounts of waste (Conesa et al., 2008). This was the period of *Sociedad Minero-Metalúrgica Peñarroya España, Sociedad Anónima* (SMMPE, SA), a company that was mainly interested by Zn and Pb, from galena and sphalerite. Nevertheless, SMMPE also exploited other minerals for given periods of time, such as pyrite to produce sulphuric acid (except for the period 1965–1973) and magnetite (from 1959 to 1967) (Oyarzun et al., 2013; Manteca et al., 2014). Small amounts of silver were also obtained as a by-product.

During the 1957–1990 open pit period (cf. Section 1), ores were treated by froth flotation, a procedure requiring the mechanical crushing and milling of rocks and minerals, in concentration plants down to small grain sizes (i.e. <180 μm in "*Lavadero Roberto*" plant, Portmán, Fig. 1), and the subsequent segregation of particles according to their physical characteristics by taking advantage of the ability of air bubbles to adhere to specific mineral surfaces in a mineral/water slurry (Kawatra, 2011; Banos-González and Páez, 2013; Oyarzun et al., 2013). Chemicals such as caustic soda, sodium cyanide, sodium ethyl xanthate, copper sulphate and sulphuric acid (Banos-González and Páez, 2013) used in the process were also added to the tailings dumped at the sea. Froth flotation allows exploiting low-grade ores economically, though it results in large volumes of tailings (Dold, 2014). Waste analyses carried out by SMMPE, S.A. (1970, 1980, 1984, 1985), showed that tailings were mainly composed of silica, phyllosilicates, iron carbonates and oxides, and other carbonates. *Minerais et métaux* (MINEMET, 1974) also identified sulphides, whereas Manteca et al. (2014) noticed high concentrations of magnetite in the mine tailings forming modern Portmán beach. The first outfall pipe was built by SMMPE in 1961, in response to

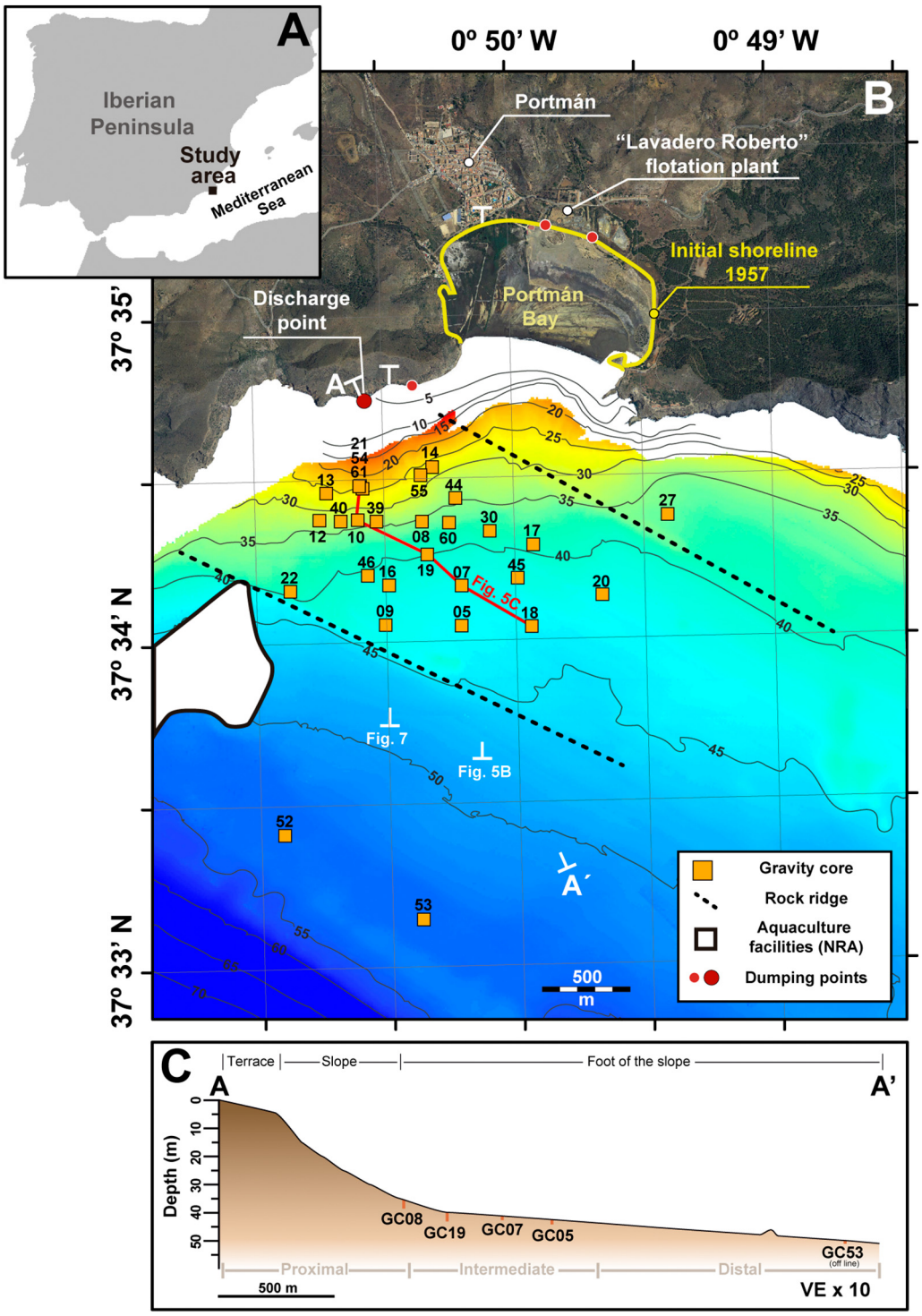

Fig. 1. (A) Location of the study area (black square) in the western Mediterranean Sea. **(B)** Detailed map of the study area showing the location of the sediment gravity cores (orange squares) investigated in this study, off Portmán Bay, in Murcia, SE Spain. The area between the initial 1957 shoreline and the present shoreline in the figure illustrates the ~600 m coastline advance due to the discharge of mine tailings. It also corresponds to the emerging part of the mine tailings deposit, much of which is underwater. Dashed black lines indicate two up to 4 m high NW-SW oriented rocky ridges crossing the study area. Location of cross sections in other figures (Figs. 5B, C and 7) is also shown. Land image is from a 2011 flight of the Spanish *Plan Nacional de Ortofotografía Aérea* (PNOA). NRA: Navigations restricted area. Isobaths in meters. Small red dots indicate second-order dumping points through time, while the biggest red dot shows the main dumping point labelled as "Discharge point" in the fig. **(C)** NNW–SSE cross section A–A' (see location in B). "Proximal" refers to the subarea from the closest to the main discharge point on the coastline and shallowest core sampling point till ~1.0–1.2 km offshore and ~ 35 m water depth, "intermediate" refers to the ~1.2–1.5 km distance range and the ~35–43 m depth range, and "distal" to the ≥1.5 km offshore and ≥43 m water depth VE: vertical exaggeration. GC: gravity core.

the need of discharging increasing volumes of mine tailings produced as a consequence of an augmentation in the amounts of ores being treated. The pipe mouth opening into the sea was placed, through time, at two locations that were about five hundred meters one from each other on the cliffs out and west of the bay ("Main discharge point" and another point east of it in Fig. 1). Of these two, the eastern outfall was in place

and kept operational during the 1961–1984 period, while the western one, or main discharge point, dumped tailings into the sea in between 1984 and 1990 from Punta Galera headland. Close to the end of the operational period, discharge rates from the later were about ~8000 to ~10000 t d^{-1} (Vilar et al., 1991; Banos-González and Páez, 2013).

Metal and metalloid contents at the top of the tailings deposit, both subaerially and underwater, are summarized in Supplementary Table 1 (i.e. ST. 1), as compiled from Benedicto et al. (2008), Peña et al. (2013) and Manteca et al. (2014) for the subaerial part, and Cerdà-Domènech et al. (2020) for the submarine one. Pb and Zn contents are noticeably high both in subaerial and underwater wastes and of the same order of magnitude in their upper bound range. According to the available information prior to the current paper, there would be significantly more As in the subaerial section (based on eight sand samples) than in the submarine one. Fe contents in the upper parts of submerged deposits are extremely high (up to 260 mg $kg^{-1} \times 10^{-3}$, or 26%), whereas Ti and Mn also show noticeable concentrations underwater. However, these two metals are not reported in the subaerially exposed section. S appears incorporated to sulphides, and Cd and Hg are either detected or, again, not reported.

3. Materials and methods

3.1. Sediment sampling

Materials and sea data used in this work were acquired mainly during oceanographic cruise NUREIEVA-MAR1 from 27/06 to 10/07/2018. One gravity core was also obtained in NUREIEV-1 cruise, from 13/03 to 24/03/2015 (ST. 2). Both cruises were carried out onboard research vessel, R/V Ángeles Alvariño from *Instituto Español de Oceanografía* (IEO) in the framework of NUREIEVA and NUREIEV research projects funded by the Spanish government.

Sediment cores were recovered by means of a 5 m long gravity corer (GC). In total, 28 gravity cores were obtained, 0.6 to 4.3 m long, resulting in 61.48 m of sediment (Fig. 1 and ST. 2). All were collected in 2018 but core GC16, which was retrieved in 2015. Gravity cores were cut and stored in 1–1.5 m in length PVC sections, resulting in 61 sections in total, 59 from year 2018 cores and 2 from 2015 core. Core sections were stored at 4–5 °C, both onboard, and during and after transportation to University of Barcelona (UB) premises, until core slicing. Additionally, short multi-corer and grab samples were also retrieved, though they have not been used in the present study.

3.2. Analytical work

3.2.1. Multiproperty continuous down core measurements

Sample characterization was carried out mainly by means of non-destructive techniques, supplemented wherever required by some destructive analyses, the later involving the grinding of discrete samples in some cases. Quasi-continuous non-destructive measurements were performed with a Geotek multi-sensor core logger (MSCL) for physical properties and an Avaatech X-ray fluorescence (XRF) core scanner for imaging and elemental composition at the CORELAB Laboratory facility of UB. Sediment core GC16 (ST. 2) was also scanned for 3D internal configuration analysis with a micro-CT scanner at the same facility.

MSCL measurements were made on non-split unaltered core sections, so that gamma-density (GD), P-wave velocity (P-WV) and magnetic susceptibility (MS) were obtained at 5 mm resolution. This resolution was considered adequate taking into account the information to be obtained as related to the time required for these types of measurements. In other words, a better resolution would have not resulted in more relevant information than the one obtained at the set measurement interval.

According to literature, there is no difference, or very minor, if GD and P-WV are measured on non-split or split sections (Gunn and Best, 1998). In case, we have measured them on whole sections, as they ensure a better preservation of sampled materials (Ross and Bourke, 2017). On the contrary, we recorded MS logs from split sections as measurements are performed by means of a point sensor (Gunn and Best, 1998; Frigola et al., 2015). Porosity (%) has been calculated according to Last and Smol (2002), assuming quartz density of 2.65 g cm^{-3} for the mineral component.

Split core sections were subsequently described after visual observation and imaged in the visible field with a high-resolution colour line scan camera mounted on the Avaatech XRF core scanner, also yielding colour parameters (CIE, La*b*) with a fixed along core resolution of 0.07 mm (70 μm) according to the camera technical characteristics. Colour values can be utilized as indicators of physical and geochemical variations thus easing the identification of facies and sedimentary structures (Debret et al., 2011).

All split core sections were scanned at 2 mm resolution with a third generation Avaatech XRF core scanner to semi-quantitatively determine the along core variability in elemental composition with the focus on metals and metalloids, to identify and characterise sedimentary facies and unit boundaries, and to distinguish natural from anthropogenic (i.e. the mine tailings) deposits and their transitions (Odhiambo et al., 1996; Sims and Francis, 2010; Boës et al., 2011; Sindern et al., 2016; Badawy et al., 2018; Busico et al., 2018; Natali and Bianchini, 2018; Banning, 2021). Such elevated resolution for XRF measurements was selected in view of the millimetre-scale internal variability of the materials in some intervals, as observed after core splitting. The Avaatech XRF core scanner provides fast, high-resolution determination of elements with an atomic mass between Al and U, and yields semi-quantitative elemental logs in counts (cts). Prior to XRF analyses, all sections were left at room temperature during 24 h to reduce water absorption in order to improve the XRF signal (Tjallingii et al., 2007). The sediment surface in each split core section was carefully covered with a 4 μm thick ULTRALENE-SPEX film to ease XRF coupling and avoid contamination. Excitation conditions were set at 10 kV, 1.0 mA without filter for 10 s, and 30 kV, 1.5 mA and a Pd-thick filter for 50 s, allowing the determination of elemental profiles of a large number of elements following Richter et al. (2006) and Rothwell and Rack (2006). A number of metals (Ca, Zr, Pb, Zn, Cu and Fe), one metalloid (As) and one non-metal (S) elements were selected as potential proxies for material sources. XRF core scanner elemental records of Pb, Zn, As, Cu and Fe were then converted to absolute concentrations using the inductively coupled plasma mass spectrometry (ICP-MS), calibrations described in Cerdà-Domènech et al. (2020), to which further ICP-MS absolute concentrations measured on 13 additional samples from core GC21 were added, thus enhancing the XRF signal-concentration ratio and strengthening calibration curves.

Micro-CT scanning was performed with an ultra-high resolution MultiTom core scanner from X-Ray Engineering (nowadays TECAN) to obtain 3D images of the internal structure of the materials and also to build 3D volumetric reconstruction of density changes. The later was achieved by using a grey colour palette, where darker and lighter zones represent lower and higher X-ray attenuation or density, respectively (Frigola et al., 2015). Scans were performed with a 0.5 mm-thick Cu filter at 90 kV, 125 W, 200 ms of exposure time and 2000 projections, resulting in a "voxel" size of 125 μm resolution.

3.2.2. Analysis of discrete samples

452 carefully selected samples from all sediment cores (ST. 2) were grain-size analysed in liquid solution with a Coulter laser particle size analyser LS230 at the Laboratory of Sedimentology of UB. This set of discrete samples was obtained from extraction of 7–9 subsamples per core section with an average length of about 1 m. Coulter laser particle size measurements provide the percentage in volume of particles from 0.04 μm to 2 mm (2000 μm) by calculating the spherical equivalent diameter of particles after measuring the angle of diffraction they cause to a laser beam (Agrawal et al., 1991). Prior to analysis, sediment samples were treated with H_2O_2 10% to eliminate organic matter, after which

one aliquot was directly analysed (bulk sample) and another one was injected with acetic acid and sodium acetate to remove carbonates (de-carbonated sample).

Main mineral phases were identified in 36 carefully selected samples by means of X-ray diffraction (XRD) on non-oriented smear slide preparations using a *PANalytical X'Pert PRO MPD Alpha1* powder diffractometer in *Bragg-Brentano* θ/2θ geometry from scientific and Technological Centres of University of Barcelona (CCiTUB), under nickel filtered Cu Kα radiation (λ = 1.5418 Å) at 45 kV and 40 mA. Minerals were identified after the X'Pert Highscore software. High Fe contents in most samples made it difficult identifying minerals low in volume (i.e. under 5 to 10%).

Total carbon (TC) and organic carbon (OC) contents were analysed on 107 selected samples using a CCiTUB, elemental organic analyser Thermo EA 1108 from Thermo Scientific, working in standard conditions (i.e. helium flow at 120 ml min^{-1}, combustion furnace at 1000 °C, chromatographic column oven at 60 °C, and oxygen loop 10 ml at 100 kPa), with a quantification limit of 0.1–0.2%, to obtain firstly inorganic carbon (IC), and secondly calcium carbonate ($CaCO_3$) contents, that were derived from equations:

$$IC = TC - OC \quad (1)$$

$$CaCO_3 = ([(IC) \times 100]/12) \times \%_{CaCO3\ in\ samples} \quad (2)$$

where 12 is the molecular mass ratio of C in $CaCO_3$.The later was obtained from each material after XRD quantification.

3.3. Other tools and sources of information

Several statistical analyses have been applied to ease the interpretation of the datasets obtained after the above-described methodologies, namely: (i) a Principal Component Analysis (PCA) and Pearson correlations on As, Ca, Cu, Fe, Pb, S, Zn, Zr, from the XRF dataset, and OC and IC from carbon.

analysis, using *Statgraphics Centurion XVIII* software, and (ii) an assessment of grain size parameters using Gradistat v.8. Software (Blott and Pye, 2001).

Historical aerial photographs from a variety of sources are used to monitor the evolution of the shoreline, the progressive infill of Portmán Bay and the occurrence of surface sediment plumes issued from the coast.

4. Results

4.1. Sedimentary facies

The exhaustive multiproxy analysis of the materials allows their characterization with a unprecedented detail, which is also unique for massive submarine mine tailings deposits resulting from the exploitation of sulphide ores. Eight distinct sedimentary facies have thus been found in the submerged extension of the mine tailings deposit of Portmán Bay, named Facies 1 to Facies 8, or F1 to F8, which encompass pre-dumping, dumping and post-dumping materials (Table 1).

Facies 1 (F1) always is stratigraphically the lowest. It consists of massive, (i.e. up to 115.3 cm thick in our sediment cores — cf. core GC27; Fig. 1 and ST. 2 —, but it is actually thicker as it continues deeper down our core bottoms), porous (47–70%), light yellowish brown (Munsell code 10Y-6/4) bimodal sandy silts and silts with shells and vegetal fibres (Table 1). Colour gradually darkens top wards, either slightly as in cores GC18 and GC52, or markedly till becoming eventually black (10YR-2/1) as in cores GC05 and GC19 (Supplementary Figures – SFs. – 1A, 1B, 1C and 2). MS is the lowest (0–150 SI × 10^{-5}) amongst all facies, whereas GD is also in the lower range of values (1.5–1.9 g cm^{-3}). Both GD and P-WV (1470–1660 m s^{-1}) show upwards-decreasing trends (e.g. Table 1 and SF. 1). The highest XRF values of Ca, one of the most abundant metals in the Earth's crust, and Zr, a transition metal, are found in this facies F1, peaking at 502 × 10^3 and 12 × 10^3 cts, respectively. Pb (0.02–27 × 10^3 cts, 40–645 mg kg^{-1}), Zn (0.16–22 × 10^3 cts, 91–501 mg kg^{-1}), As (0–14 × 10^3 cts, 70–1089 mg kg^{-1}), Cu (74–404 cts, 2–634 mg kg^{-1}), S (2–11 × 10^3 cts) and Fe (11–394 × 10^3 cts, 2–20%) contents, as obtained directly from XRF measurements and after calibration, are in the lower range of values compared to the other facies identified. Vertical trends are either lacking or appearing in some cores for some elements only (i.e. Zn, As and Fe), as illustrated by cores GC18 and GC19 (SFs. 1C and 2), which show slightly upwards increasing trends for those elements. The main minerals in F1 are calcite and quartz in about the same proportion. Secondary minerals are dolomite and aragonite, with some phyllosilicates (e.g. muscovite, biotite, clinochlore) and occasional pyrite mostly in the facies top as also shown by slightly rising Fe contents (SFs. 1B, 1C and 2). F1 shows both the highest OC (0.64–2.07%), IC (4.65–8.78%) and $CaCO_3$ (32.2–60.7%) values amongst all facies. It has been recovered in intermediate and distal locations within the study area, though it likely occurs in proximal locations as well, where it would lay too deep in the sedimentary sequence to be reachable by our gravity cores.

Facies 2 (F2) appears in cores from the intermediate and distal, deeper reach of the study area, above F1. It consists of homogeneous to mm to cm thick semi-laminated, porous (48–71%), dark greyish brown (2.5YR-4/3 – 10YR-3/2) bimodal silts with occasional orange layers (10YR-4/6) and black patches, as observed in cores GC05 and GC19 (SFs. 1A and 2), and also in other cores such as GC60 and GC46. F2 presents very small, isolated fragments of shells, and vegetal fibres are also observed, but they are much less abundant than in F1. GD is similar to slightly lower (1.5–1.8 g cm^{-3}) than F1, similarly to P-WV (1455–1620 m s^{-1}). MS is clearly higher (0–6000 SI × 10^{-5}) than in F1, with the highest values usually corresponding to the above-mentioned orange layers. None of these three parameters (GD, P-WV and MS) shows any trend. F2 is rather rich in Ca (20–393 × 10^3 cts) and Zr (0.7–11 × 10^3 cts), though slightly below F1. This facies shows significant increments, though in varying degrees, of all metals and metalloids compared to F1, but especially in Pb and Cu. The range of values is 1–141 × 10^3 cts (58–3455 mg kg^{-1}) for Pb, 0.7–42 × 10^3 cts (91–501 mg kg^{-1}) for Zn, 0.2–31 × 10^3 cts (90–932 mg kg^{-1}) for As, 0.1–1.3 × 10^3 cts (95–2755 mg kg^{-1}) for Cu, and 30–570 × 10^3 cts (2–29%) for Fe. The highest values mostly coincide with the orange layers, which can be used as key horizons in different cores containing this facies. Element S displays values (2–28 × 10^3 cts) that are only slightly higher than in F1. Main minerals in F2 are calcite and quartz in similar proportions, followed by dolomite, phyllosilicates (e.g. muscovite, biotite, fraipontite, greenalite or clinochlore), and smaller quantities of sulphides (e.g. pyrite, covellite or sphalerite), Fe-Mn oxides (e.g. magnetite or bixbyite), Fe-carbonates (e.g. siderite or ankerite), and Zn silicates, which fits with the observed increase in metallic elements compared to F1. There is no apparent relation between mineral composition and colour changes. OC, IC, and $CaCO_3$ contents range from 0.51 to 1.83%, 1.22 to 7.78%, and 7.3 to 46.7%, respectively.

As for F1, F2 has been core sampled in intermediate and distal locations since there the cumulative thickness of overlying facies is less compared to proximal areas. F1 and F2 are easily distinguishable one from each other as shown by changes in XRF elemental records, especially metals, at their contact, amongst other properties (e.g. strong diminution of shell fragments and vegetal fibres) (Table 1). Vertically, these two facies are always associated, with F1 occurring systematically under F2. The nature of their contact ranges from abrupt (e.g. GC05; SF. 1A) to gradual (e.g. GC18 and GC19; SFs. 1B and 2). Nevertheless, F2 is lacking or poorly developed in some cores. When this happens, the top of F1 presents high contents of metals and metalloids (e.g. GC07 and GC20), which suggest a condensed F2.

Facies 3 (F3) forms the bulk of most cores located up to 1.5 km from the shoreline main discharge point in different directions (Fig. 1) and, therefore, is widespread. It appears always atop of F1 or F2. F3 has

Table 1
Description and summary of physical and chemical properties of the eight sedimentary facies identified in the up to 4.3 m long sediment cores analysed in this study (Supplementary Table 2). Facies are numbered from F1 at the bottom to F8 at the top. Facies F3, F4, F5 and F6 may appear at different stratigraphic positions, alternating one to another. Main diagnostic properties, values and trends per facies are in bold. Colour and grain size classifications are after the Munsell colour chart and Gradistat, respectively. Wherever judged appropriate some facies sharing given ranges of variability or trends for specific properties have been grouped for ease of description. CaCO3: calcium carbonate, as calculated from XRD data for each facies and facies grouping. Cts, counts. GC, gravity core; GD, gamma density. IC, inorganic carbon. MS, magnetic susceptibility. OC, organic carbon; SF., supplementary figure; ST., supplementary table. Mineralogy: Ank, ankerite; Arg, aragonite; Cal, calcite; Dol, dolomite; Fe-Ox, iron oxides; Mag, magnetite; Phyll, phyllosilicates (biotite, clinochlore, greenalite, fraipontite, muscovite, phlogopite…); Py, pyrite; Qz, quartz; Sid, siderite; Sulph, sulphides (sphalerite, arsenopyrite, covelline…); Zn sil, Zn-silicates. In the Mineralogy row, 1) refers to dominant minerals, whereas 2) refers to accessory minerals. Bell-shaped refers to the graphic's morphology similar to a bell or half bell shape.

Facies	F1	F2	F3	F4	F5	F6	F7*	F8
Description	**Massive light yellowish** brown **sandy silts and silts**, with abundant **vegetal fibres and shell fragments.** Organic matter rich black top	**Massive to** mm to cm **thick semi-laminated dark greyish brown silts** with **black patches**. Some **orange coloured layers**, vegetal fibre s and shells	Mm to cm **laminated multicoloured muds, silts and sands,** with predominance of olive tones. Also other sedimentary structures	Massive olive to olive black **fining upwards silts and sandy silts**, with occasional cross-laminations at the facies top	**Homogeneous olive grey silts**	**Massive to semi-laminated multicoloured silts** with predominance of olive tones	**Massive to semi-laminated dark grey silts** with bioturbation marks	**Massive dark grey to black sandy silt**s and fine sands with signs of bioturbation
Munsell colour codes	10Y-6/4 10YR- 2/1	2.5YR-4/3 10YR-3/2 Orange layers 10YR-4/6	5Y and 5YR 10YR-3/1, -2/1	5Y-4/3 5Y-2.5/1	5Y-4/2	5Y	5Y-4/1	5Y-3/1 5Y-2.5/1
Grain size distribution	Bimodal	Bimodal	**Polimodal**	Polimodal	Unimodal	Bimodal	Polimodal	Unimodal
Mean grain size (μm)	10 and 60	11 and 25	15, 25 and 70	20, 35 and 150	20	10 and 40	20, 30 and 80	50
Classification after grain size	Sandy silts	Silts	Silts to fine sands, some clays	Silts and sandy silts	Silts	Silts	Silts and fine sands	Sandy silts to fine sands
Gamma density (GD) (g cm^{-3})	1.5–1.9	1.5–1.8	1.5–2.2	1.6–2.2	2.0–2.2	1.5–2.0	1.9–2.1	1.8–2.0
GD per grain size (g cm^{-3})	–	–	Silts 1.5–1.9 Sands 1.9–2.2	Silts 1.6–2.0 Sands 2.0–2.2	–	–	–	–
GD grouping F3-F6 (g cm^{-3})	–	–	1.5–2.2				–	–
GD trends	**Upwards decreasing**	No trends, rather uniform	No trends, uneven	**Bell-shaped** (i.e. upwards increasing till peaking and then decreasing)	**Mostly uniform** with no trends, and **values in the high range (≥2.0 g cm^{-3})**	Rather uniform, no trends	Upwards decreasing	No trends
P-wave velocity (m s^{-1})	1470–1660	1455–1620	Most commonly 1450–1500; 1550–1600 in sandy layers				1480–1630	1440–1630
P-wave velocity trends	**Upwards decreasing**	No trends, rather uniform	No trends, with spikes in sandy layers	**Smooth bell-shaped pattern**	**Mostly uniform**	Mostly constant (~1490 m s^{-1})	Bell-shaped patterns	No trends
MS (SI × 10^{-5})	0–150	0–6000	100–9300, with highest values in magnetite-rich sandy and silty layers/intervals				90–3000	4–3300
MS trends	Essentially uniform, low values	From rather uniform to uneven, depending on sediment core	Heterogeneous, uneven	**Bell shaped pattern**	**Mostly uniform within high range (3000 SI × 10^{-5}),** with no trends	From rather uniform to uneven, depending on sediment core	Rather uniform	
Porosity (%)	47–70	48–71	23–70	24–64	31–55	37–70	36–68	34–69
Ca (cts × 10^3)	**92–502**	20–393	7–261	13–210	33–92	23–224	17–92	25–220
Zr (cts × 10^3)	**2–12**	0.7–11	0.3–5	0.6–5	0.6–3	0.5–6	1.0–6	1–7
Ca and Zr trends	No trends	Succession of uniform and fluctuating intervals, with lowest values in orange coloured layers	Noticeable fluctuations in Ca. The upper bound range of values is lower than in F1 and F2				Some fluctuations, mainly in Ca.	
Pb (cts × 10^3)	0.02–27	**1–141**	2–59	3.5–46	6.5–18	4–27	4–13	4–14
Pb (mg kg^{-1})	40–645	**58–3455**	40–1433	60–1104	136–415	80–647	69–288	68–323
Zn (cts × 10^3)	0.2–22	0.7–42	**3–45**	3–38	16–26	4–32	2–10	8–45
Zn (mg kg^{-1})	91–501	90–932	**91–1007**	91–846	351–574	98–706	231–793	171–990
As (cts × 10^3)	0–14	0.2–31	**0.3–38**	1.3–27	3–10	0.5–11	9–36	1–14
As (mg kg^{-1})	70–1089	101–2213	**95–2755**	179–1964	307–794	92–874	204–808	164–1051
Cu (cts × 10^3)	0.07–0.4	**0.1–1.3**	0.08–0.9	0.1–0.6	0.1–0.5	0.1–0.4	0.1–0.4	0.1–0.3
Cu (mg kg^{-1})	2–634	**95–2448**	22–1688	57–1054	79–742	42–709	57–602	34–529
S (cts × 10^3)	2–11	2–28	**2–140**	5–70	9–39	2.6–19	4–50	4–91
Fe (cts × 10^3)	11–394	30–570	81–621	**141–636**	291–560	70–544	203–476	171–446
Fe (%)	2–20	2–29	4–31	**7–32**	15–28	4–27	10–24	9–23

(continued on next page)

Table 1 (*continued*)

Facies	F1	F2	F3	F4	F5	F6	F7*	F8
Mineralogy	1) Cal, Qz 2) Dol, Arg, Phyll, Py	1) Cal, Qz 2) Dol, Phyll > Sulph, Fe-Ox, Sid, Zn Sil.	1) Qz, Py, Sid, Ank, Mag, Fe rich phyll, 2) Cal, Dol, Sulph, Zn-sil.				1) Qz, Phyll, Py 2) Cal, Sid, Dol, Mag, Sulph	
OC (%)	0.64–2.07	0.51–1.83	0.13–1.28				0.25–0.87	
IC (%)	4.65–8.78	1.22–7.78	1.15–3.97				0.51–2.47	
$CaCO_3$ (%)	32.2–60.7	7.3–46.7	2.4–8.3				1.9–9.3	
Representative sediment cores (cf. Fig. 1, ST. 2)	GC05, GC18, GC19, GC20, GC27, GC52	GC05, GC17, GC19, GC45	GC08, GC19, GC22, GC55, GC61	GC05, GC10, GC12	GC16, GC19, GC30	GC18, GC20, GC52, GC53	GC19, GC40	
Occurrence within the study area	Intermediate to distal	Intermediate to distal	Proximal to intermediate	Proximal to distal	Intermediate	**Distal**	Proximal to distal	
Figures	Fig. 2 and SFs. 1 and 2	Fig. 2 and SFs. 1 and 2	Fig. 2 and SFs. 1 to 4	Fig. 2 and SFs.1, 3 and 4	Fig. 2 and SFs. 2 and 4	Fig. 2 and SF. 1	Fig. 2 and SFs. 2 and 4	

been identified down to 4.31 m core depth (e.g. core GC21). It consists of multicoloured, laminated, polimodal silts and sands. Laminations are from mm to cm scale, and are associated with colour changes, mainly in the finer grain sizes (silts and muds), and to grain size changes (silts and sandy silts interstratified with silty sands and sands), as illustrated by cores GC19 and GC61 (SFs. 2 and 3). Muddy and silty layers display a wide range of colours, mostly in the olive, orange and greyish tones (5Y and 5YR mainly), while coarser grained layers present dark tones (e.g. 10YR-3/1), where black is common occurrence (e.g. 10YR-2/1). Lamination faints south-eastwards towards the edge of the study area. Shells are absent, and vegetal fibres have been rarely found. Physical properties in F3 fluctuate noticeably (GD: 1.5–2.2 g cm^{-3}; P-WV: 1450–1550 m s^{-1}; MS: 500–8200 SI $\times 10^{-5}$; porosity: 23–70%). Sharp increases in physical properties are commonly associated to black silty and sandy layers, especially for GD and MS. Contents of Ca (7–261 $\times 10^3$ cts) and Zr (0.3–5 $\times 10^3$ cts) are often lower than in F1 and F2 (Table 1). In contrast, contents in elements such as Zn (3–45 $\times 10^3$ cts, 91–1007 mg kg^{-1}), As (0.3–38 $\times 10^3$ cts, 95–2755 mg kg^{-1}), S (1.6–140 $\times 10^3$ cts) and Fe (81–621 $\times 10^3$ cts, 4–31%) are most commonly higher than those observed in F2 and F1, whereas Pb (2–59 $\times 10^3$ cts, 40–1433 mg kg^{-1}) and Cu (0.08–0.9 $\times 10^3$ cts, 22–1688 mg kg^{-1}) are in medium - lower range of values regarding F2.

Facies 4 (F4) consists of massive olive to olive-black (5Y-4/3 – 5Y-2.5/1) polimodal silts and sandy silts forming a fining upwards sequence, as observed for instance in cores GC05, GC61 and GC16 (SFs. 1A, 3 and 4 respectively) or also GC10 and GC12. Physical properties increase upwards gradually till peaking to then decrease again, thus leading to bell or half bell shaped curves. This is especially in the case of GD, as illustrated by core GC18 (SF. 1B), where this parameter peaks at 2.1 g cm^{-3} to then drop back to 1.7 g cm^{-3}. PW-V and MS also show this pattern along F4 though it is occasionally smoothened. Porosity in F4 (24–64%) is in the same range than F3. Element contents and patterns are similar to those in F3 (Table 1). F4 appears along the entire range of locations, i.e. from proximal to distal.

Facies 5 (F5) is made of massive olive grey (5Y-4/2) unimodal silts. Physical properties show low variability, with high and uniform values in GD (≥2 g cm^{-3}) and rather high values in MS (~3000 SI $\times 10^{-5}$), as illustrated for instance by cores GC19 (SF. 2) and GC16 (SF. 4). GD and MS make F5 somehow unusual as higher bound values in other facies commonly correspond to sandy silts and sands, whereas in F5 they correspond to silts. In contrast, PW-V does now show particularly high values but is rather uniform. Porosity range is narrower (31–55%) than for instance F3, F4 and F6, and about equal than to F2. Elemental contents also vary within forks that are narrower than in F3 and F4 (Table 1). F5 usually appears in intermediate locations, although we cannot discard another situation.

Facies 6 (F6) is made of massive to semi-laminated multicoloured, with dominating olive tones (e.g. 5Y), bimodal silts as observed, amongst other, in cores GC18 and GC52 (SFs. 1B and 1C), and also GC20, GC53 and GC27. F6 physical properties are quite similar to F3, though generally linear and in the lower bound range, with 1.6–2.1 g cm^{-3} for GD, P-WV close to 1490 m s^{-1}, and around 1000 SI $\times 10^{-5}$ for MS, as observed in cores GC18 and GC52 (SFs. 1B and 1C). In some cores, though, MS displays larger variability, from 200 SI $\times 10^{-5}$ to 5000 SI $\times 10^{-5}$ (e.g. core GC20). Element contents are similar to those in F3 and F4, with the exception of S (2.6–19 $\times 10^3$ cts), which is close to the range of values in F1 and F2 (Table 1). F6 is common in distal locations within the study area.

F3, F4 and F5 have been identified up to ~1.4–1.5 km south of the main discharge point on the shoreline and down to 43 m depth (Fig. 1), and they appear in association in our cores. F6 extends slightly farther and deeper than F3 to F5, up to more than 1.6 km south of the main discharge point and down to 45 m depth south-westwards or even 53 m depth to the south (e.g. GC52; SF. 1C), but also north of the northern rocky ridge referred to in Section 2.1, as observed in core GC27 (Fig. 1). F3, F4, F5 and F6 are easily distinguishable from each other visually, and even more by using micro-CT images (SF. 4). Micro-CT images show the laminated character of F3, which is often interbedded with F4, as evidenced by differences in grey colour scale, together with sedimentary structures, such as cross-laminations, microfractures and other internal deformation structures like contorted layers and core-scale flame structures. F4 is seen in micro-CT images as non-laminated with subtle gradual hue changes in the grey scale and cross laminations at the facies top. Finally, F5 is seen as homogeneous intervals with middle tones in the grey scale (SF. 4).

Visual characteristics and internal configuration correlate with physical properties, which variations generally relate to grain size changes as well. Nevertheless, distinguishing F3, F4, F5 and F6 from their chemical properties is not so obvious given the noticeable internal heterogeneity they present, with frequent small-scale changes. These four facies, F3 to F6, share a noticeable decrease in Zr, compared to F1 and F2, whereas Ca contents are shifted towards the middle-lower range, also with respect to F1 and F2 (Table 1). However, they are close to those of F7 and F8 (see further down). In addition, those four facies display fluctuating contents of the other elements measured, from Pb to Fe, with peak values that are amongst the highest for Zn (up to 45 $\times 10^3$ cts, 1007 mg kg^{-1}), As (up to 38 $\times 10^3$ cts, 2755 mg kg^{-1}), S (up to 140 $\times 10^3$ cts) and Fe (up 636 $\times 10^3$ cts, 32%), mostly in facies F3 (Table 1). On the contrary, Pb and Cu peak values are lower than those in the underlying facies F2 (Table 1). Whereas the same set of facies, F3 to F6, commonly displays colour changes from one layer to another, mineralogical differences are scarcely relevant according to XRD analyses. Main mineral is quartz, followed by Fe-rich minerals such as pyrite, siderite, ankerite, magnetite and Fe–phyllosilicates (e.g. clinochlore, greenalite and biotite). The same mineral suite has been found in the sands of Portmán beach (Manteca et al., 2014), where hematite and Fe silicates have been described as well. Calcite, dolomite, Zn-silicates, and other sulphides as

sphalerite or even arsenopyrite are present as secondary minerals. Samples from these facies display OC contents ranging from 0.13 to 1.28%, whereas IC ranges from 1.15to 3.97%, which is less or is in the lower range of values observed in underlying facies F2 and F1 (Table 1). $CaCO_3$ contents range from about 2.4 to 8.3%, which again is less or is in the lower range of values found in F2 and F1 (Table 1).

Facies 7 (F7) is made of massive to semi-laminated (especially in the lower part of the facies) dark grey (5Y-4/1) polimodal, bioturbated silts and fine sands (Table 1). Porosity usually is in the 36–68% range, which is close to F5 and, especially, F6. F7 appears under F8 (see further down) and is quite rare, as it has been found in few cores (e.g. GC19 and GC16; SFs. 2 and 4). Concerning physical properties, whereas GD does not vary much (1.9–2.1 g cm^{-3}), P-WV oscillates within the 1480–1630 m s^{-1} range, which is similar to the one in previously described facies. MS shows a range of values (90–3000 SI $\times 10^{-5}$) that is narrower than in F2 to F6 and wider than in F1 (Table 1). The range of variation and peak Ca contents (17–92 $\times 10^3$ cts) is lower than in any other facies but F5. Peak Zr contents (1–6 $\times 10^3$ cts) are higher than in F3 to F5 and equal to those in F6 (Table 1). Zr increase with respect to the materials below can be rather pronounced, as seen for instance in core GC19 (SF. 2). Pb, Zn and As contents are generally lower than in underlying facies, while Cu, S and Fe could be either higher, similar or lower than in previously described facies, also depending on the specific facies considered for comparison (Table 1). For example, the fork for Cu contents (0.1–0.4 $\times 10^3$ cts, 57–602 mg kg^{-1}) is rather similar to most other facies but F3 and, especially, F2. The fork for S contents (4–50 $\times 10^3$ cts) is more or less close to those in F3 to F5, and clearly reaches higher values than in F6, F2 and, in particular, F1. Finally, the range of variation for Fe contents (203–476 $\times 10^3$ cts, 10–24%) is of about the same order than in F2 to F6, with a higher lower bound than F2, F3, F4 and F6, and a lower upper bound than F2 to F6. The variation fork of F1 is the only one that is lower than F7 both in their lower and upper bound (Table 1). Mineralogy is dominated by quartz, phyllosilicates (namely clinochlore and biotite) and pyrite, with calcite, siderite, dolomite, magnetite, sphalerite and arsenopyrite as secondary minerals. Phyllosilicate peaks are sometimes pronounced.

Facies 8 (F8) consists of massive dark grey (5Y-3/1) to black (5Y-2.5/1) unimodal sandy silts and fine sands with signs of bioturbation. The porosity fork (34–69%) is about the same than in F7, with a dominance of the higher values within that range. F8 appears at the top of most sediment cores, such as GC05, GC18 and GC19 (SFs. 1A, 1B and 2). Where lacking it is likely because of the loss of the uppermost centimetres of the sedimentary sequence while coring, as it sometimes happens with gravity corers. Physical properties, which are close to those in F7, do not show any particular trend. In terms of element counts, F8 is very similar to F7, with about the same range of variation for the various elements but Ca (25–220 $\times 10^3$ cts), Zn (8–45 $\times 10^3$ cts, 171–990 mg kg^{-1}) and S (4–91 $\times 10^3$ cts), which values are most often higher in F8. Zr (1–7 $\times 10^3$ cts) tends to increase upwards, either progressively or sharply till reaching values similar to those in F1 and F2,

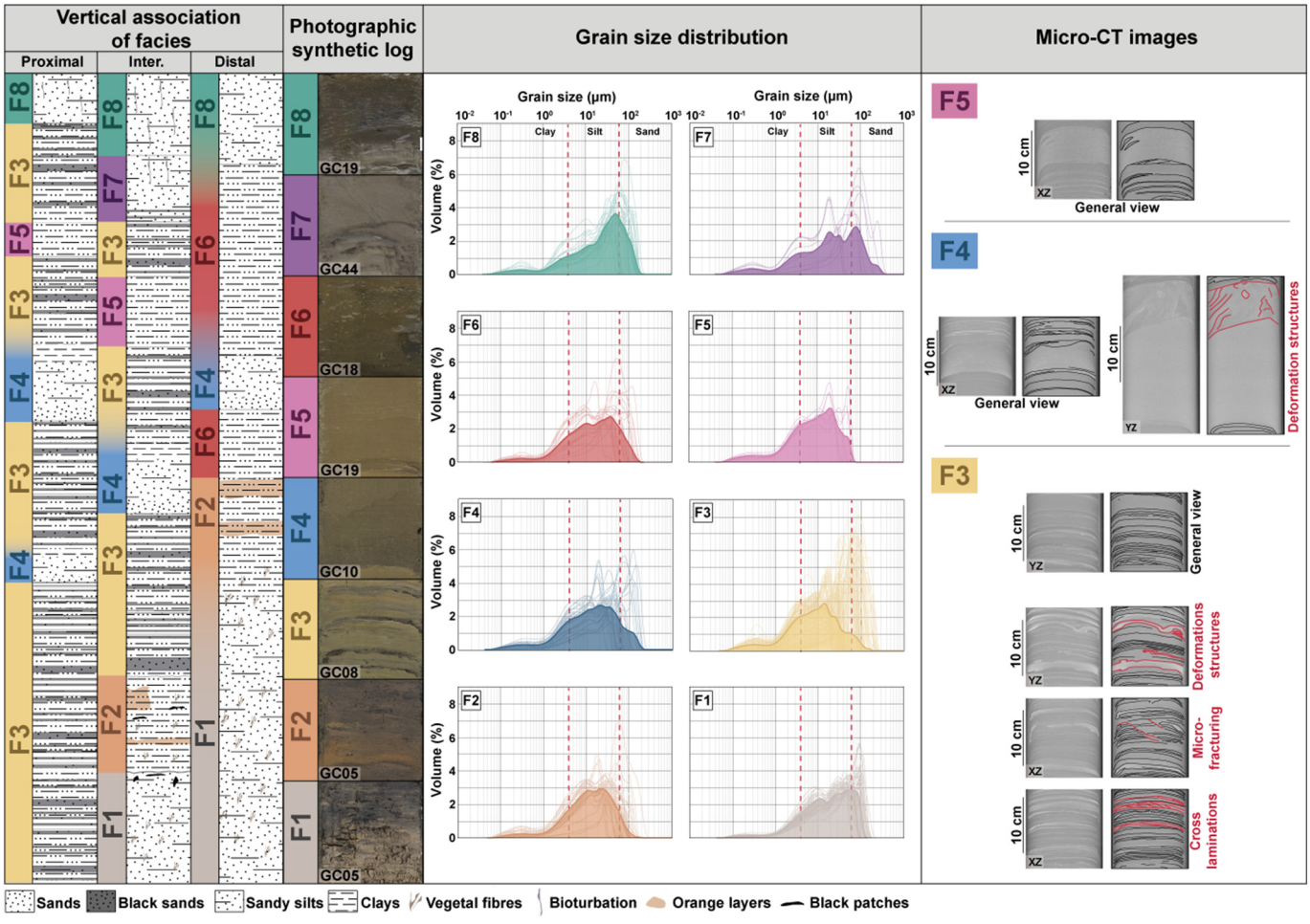

Fig. 2. Graphic synthesis of the eight facies (F1–F8) identified in the area occupied by the submarine extension of the mine tailings deposit of Portmán Bay including synthetic logs of the vertical association of facies in proximal, intermediate and distal locations (not to scale), photographs of the facies in wet condition following core splitting, grain size distribution plots, and micro-CT images and their interpretation showing the internal configurations and sedimentary structures within facies F3, F4 and F5. In the interpreted micro-CT images, distinctive sedimentary structures and laminations are marked by red and black lines, respectively. This figure is to be viewed together with Table 1.

at least in some cores (SFs. 1, 2 and 4). As for F7, OC ranges from 0.25 to 0.87% and IC from 0.51 to 2.47%, which are not far from the overall range of variation found in F3 to F6 but are lower than in F1 and F2 in most subsamples. The fork for $CaCO_3$ contents (1.9–9.3%) shows, jointly with F7, the lowest range within the identified set of facies.

Fig. 2 is a graphic synthesis of the eight facies (F1 to F8) described above, which complements Table 1 and brings in additional information, including synthetic logs of the vertical association of facies in intermediate and distal locations within the study area, photographs of the facies in wet condition as they appear in split core sections immediately after core opening, grain size distribution plots showing the unimodal, bimodal or polimodal character of the samples from each facies, and micro-CT images visualizing internal configurations and sedimentary structures within selected facies, namely F3, F4 and F5.

As shown in the synthetic logs, F1 and F2 always appear in this order from bottom to top and underlie all the other facies, whereas F8 always caps the sedimentary sequence in the retrieved cores if not lost during coring. When present, F7 underlies F8. On the contrary, F3 to F6 may appear interbedded at different levels in the sedimentary sequence and one or more of them may lack in given cores and locations (Fig. 2).

4.2. Bay infill and shoreline evolution

A set of historical aerial photographs from 1956 to 2019 provides information on the pre-dumping state of Portmán Bay and on its progressive infill and associated shoreline advance till reaching its current state, and illustrates the persistence through time of sea surface suspensate plumes because of human activities linked to mining (Fig. 3).

The oldest photograph shows the original shape of Portmán Bay, with a small quay and a vessel loading pier to the west and centre of the bay, respectively. There are also some clearly visible floating suspensate plumes in the inner bay (Fig. 3A). The second image is from 1974 (i.e. 18 years after the beginning of mine tailings dumping into the sea) and shows how the tailings that had been discharged off bay ended to a large extent into it thus leading to a first period of infill mostly of the inner and western part of the bay. Floating particle plumes are clearly visible in and off bay, and the former quay and pier became useless as they got entirely surrounded by emerging tailings (Fig. 3B). The photograph from 1984 shows how infill has progressed from one side to the other of the bay, including some clearly visible accreting lines (Fig. 3C), which are indicative of a high-supply, wave dominated sedimentation pattern (Bridge and Demicco, 2008), as previously suggested by Pauc and Thibault (1976) in their pioneering study of the infill of Portmán Bay by mine tailings.

The 1999 image, which post-dates by 9 years the cessation of dumping operations, illustrates the complete infill of the bay and the persistent triggering of suspensate plumes issued from the artificial mine waste shoreline (Fig. 3D). The 2011 photograph further shows suspensate plumes and some smoothening of the artificial coastline jointly with, again, a nice succession of accretion lines and some signs of re-vegetation on the leftmost part of the bay and of human intervention (whitish area) in its innermost part (Fig. 3E). The most recent aerial view, dating from 2019, illustrates the intensification of human intervention on the emerged part of the mine tailing deposits within the bay, as shown by car trails and bounded sections including a shallow pool in greenish colours extending from side to side of the bay, parallel to a narrow, artificially upraised beach levee (Fig. 3F). Such an intervention was part of a remediation plan that was stopped shortly after its start due to lawsuits.

5. Discussion

5.1. Element sources and their associations as proxies for the interpretation of sedimentary facies

Devising the sources of metals (Ca, Zr, Pb, Zn, Cu and Fe), metalloids (As) and non-metals (S) in the investigated facies, and assessing their respective relationships, is a way to ascertain the origin of the facies themselves and of stratigraphic units in the investigated deposits. Element contents and distributions in the tailings themselves should mainly result from open pit mining, ore treatment and tailings discharge to the sea, eventually followed by post-depositional processes.

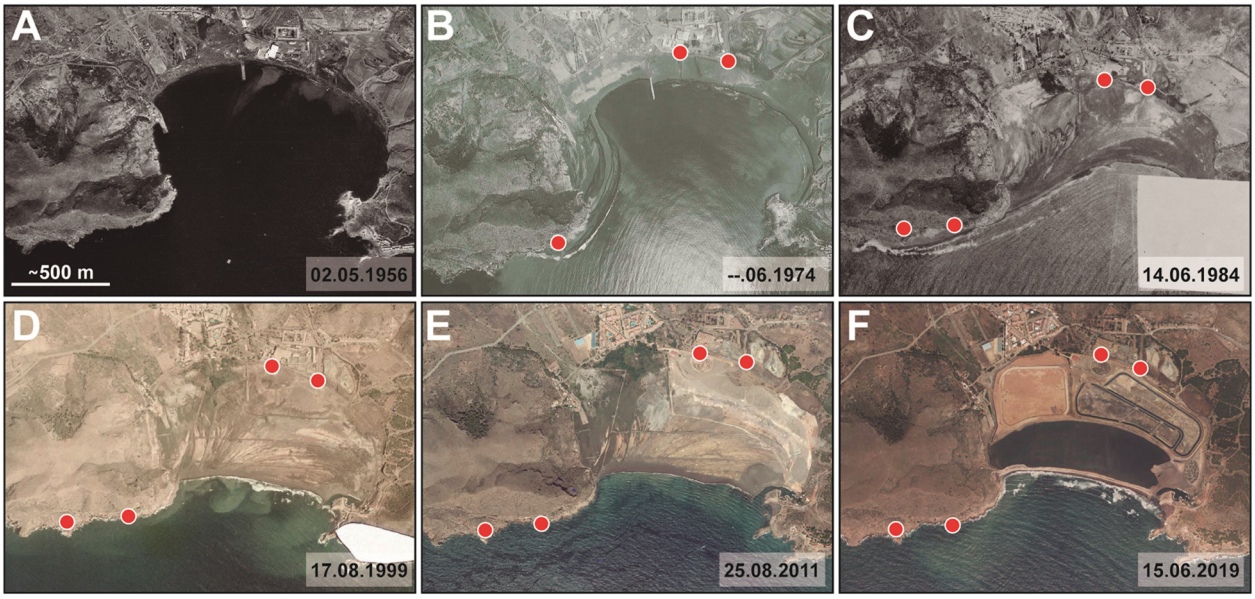

Fig. 3. Succession of aerial photographs (A, B, C, D, E and F) from 1956 (pre-dumping) to 2019 illustrating the infill of Portmán Bay and the evolution of the shoreline, jointly with human interventions in the post-dumping period. Note the presence of floating particle plumes in most images. Portmán village and what is left from "*Lavadero Roberto*" are clearly visible on the upper left corner of images E and F, and east of the village, respectively, and can be also spotted in the rest of images though not so easily. Images D, E and F show close to its lower right corner a curved waterway giving entrance to a small harbour used by locals, which was built after the dumping period. The squared and oblong white areas in the lower right corner of images C and D are intended to protect military installations from view. Photographs are from various sources and have been extracted from open access *Fototeca Digital del Centro Nacional de Información Geográfica* of Spain, except for image F, which has been downloaded from *Google Earth Pro*. Red dots mark mine tailings outfalls used through time. The main one is the westernmost, outside of the bay itself (labelled "Main discharge point" in Fig. 1). See main text for further details.

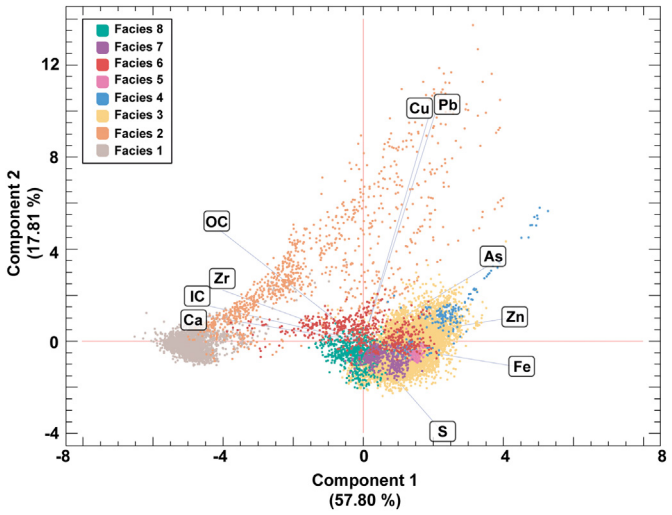

Fig. 4. Scatter plot obtained from a Principal Component Analysis (PCA) for As, Ca, Cu, Fe, Pb, S, Zr and Zn after 14,601 XRF data points, and OC and IC%. Coefficients for the two principal components are shown in Supplementary Table 3.

The question is to which point element contents and their associations are diagnostic in discriminating how the different facies formed and what each of them represents.

To that end a PCA and Pearson's correlation were applied to 14,601 data points from XRF elemental profiles of the above-mentioned elements together with OC and IC data (Fig. 4 and ST. 3).

The scatter plot of the two first components, PC1 and PC2, explains 75.61% of the total variance. PC1 (57.80% variance, horizontal axis) shows that all elements but Ca, Zr, OC and IC are grouped on the positive side of the plot (i.e. they are positively correlated) and they are strongly correlated between each other (ST. 3). On the positive side, the strongest correlations are those of Fe and Zn ($r = 0.80$), and Cu and Pb ($r = 0.75$). The only negative correlation amongst elements other than Ca and Zr with respect to the rest of elements is between Pb and S, but its value is very small (ST. 3). The second component (17.81% variance, vertical axis) places Pb, Cu and As and Zr, and OC, in clearly positive values while S is in the negative side. Ca and IC, and Zn and Fe are in intermediate positions, close to PC2 axis.

The PCA plot also shows how distinct F1 and, to a lesser extent, F2 are from the rest of facies (F3–F8), most of which data points form a rather compact cluster around the crossing of PC1 and PC2 axes (Fig. 4). Such a distribution is similar to the one found by Odhiambo et al. (1996) in a British Columbia coastal fjord where mine tailings from metallic ores had been dumped as well. It is to be noted that F2 shows a noticeable dispersion of its data points, from the location of F1 to the right and upwards, which is indicative of a transitional character between F1 and the rest of facies grouped in the main cluster. Data points from F7 and F8 appear in a rather compact distribution, to the right of the F1 cloud, thus indicating some affinities between them. This could be viewed as an incipient trend for F7 and F8 records to approach the one of F1. F6 instead shows a larger dispersion though not as pronounced as for F2. F3 and F4 also display some scattering to the right and upwards, which is indicative of internal variability. Overall, though with some overlaps, F3 to F8 occupy well–defined areas within the main cluster (Fig. 4), which supports them being considered as distinct facies.

Elemental contents and distribution can be used to distinguish geogenic from anthropogenic inputs in areas where natural sedimentation has been disturbed by human action, as is the case for Portmán Bay. Namely, Zr and Pb have been used previously as proxies for geogenic and anthropogenic inputs, respectively, in lake sediments (Boës et al., 2011). Zr is mainly present in mineral zircon ($ZrSiO_4$), and is insoluble, immobile, weathering-resistant, not utilized biologically, and lacks relevant anthropogenic sources (Hayashi et al., 1997; Koinig et al., 2003). In our case, Ca, IC and carbonates can also be considered as good geogenic proxies as, previous to dumping of mine tailings, sedimentation in the study area was dominated by $CaCO_3$ deposits, as still is in nearby areas. This fits with the high contents of Ca and carbonates in F1 and, to a lesser extent, in F2 (Table 1). Ca and carbonate contents in F3 to F8 are attributed to minerals such as mainly siderite but also calcite and dolomite (Table 1). Therefore, taking Ca and Zr, and also $CaCO_3$ contents, as geogenic proxies allows clearly differentiating F1 and F2 from the rest of facies.

Elements such as Pb, Zn, As, Cu and Fe, which are significantly present in the mined ores, represent anthropogenic inputs and, therefore, their presence in noticeable amounts in any given facies is indicative of human-mediated sedimentation. It should be noted that some of them show rather high correlation coefficients, such as those already pointed out for Fe-Zn and Cu-Pb, but also Fe-As ($r = 0.60$), and Zn-As ($r = 0.68$) (ST. 3). S has low to very low correlation coefficients, either positive or negative, with all other elements, though it is commonly more abundant in facies F3 to F8 than in F1 and most often F2 (ST. 3), as it could be expected in deposits resulting from the mining of sulphide ores.

From the geochemical viewpoint, F2 is particularly interesting as it shares physical and chemical characteristics that make it similar to F1 (e.g. OC contents, and also quite high contents of Ca and Zr) but also to some of the other facies, as it presents similar (e.g. Zn, As, Fe) or even higher contents (e.g. Pb and Cu) of anthropogenic elements with respect to individual facies from F3 to F8 (Table 1). Therefore, F2 should be considered a transitional facies marking the shift from natural sedimentary conditions represented by F1, as indicated by geogenic proxies, to human-disturbed conditions, represented by facies atop of F2, as shown by anthropogenic proxies.

One interesting aspect is how elements under scrutiny relate to OC in the different facies. It is well known from literature that heavy metal (i.e. Pb, Zn, Cu, Fe) and metalloid (i.e. As) contents have a strong affinity with organic matter and clay minerals, which can also play a major role in their segregation (Warren and Haack, 2001; Twardowska and Kyziol, 2003; Dou et al., 2013; Sindern et al., 2016; Delshab et al., 2017). Most of our facies are dominated by silts with varying proportions of fine sands and clays (Fig. 2 and Table 1), including the mine tailings. The minority character of clays in the deposit could be either because they were produced in rather small amounts during ore crushing or because the clay fraction was washed away by coastal hydrodynamics before final particle settling, or because of a combination of both processes. Crushing caused minerals usually appearing as coarse grains, such as quartz or magnetite, to be part of the finer fractions dominating the deposits, namely silts and fine sands (Table 1).

Correlation between the elements under consideration and OC in all facies and in F2 alone further shows the distinct character of the later (ST. 3). OC shows positive correlation with Ca ($r = 0.80$) and Zr ($r = 0.76$), i.e. the two geogenic proxies, and a negative correlation with heavy metals, especially Fe, Zn and As ($r = 0.79$, 0.65 and 0.47, respectively) (ST. 3). However, when looking at data points from F2 only, it appears that there is no relevant correlation of OC with the above, in contrast with all other facies (ST. 3). This would indicate that segregation and accumulation of heavy metals in F2 was driven by processes and mechanisms other than those controlling their presence in the facies above. These can only be sedimentary processes during the initial stages of dumping or changes in ore treatment, or a combination of both. It is to be recalled here that both peak values of Pb and Cu are reached within F2 (Table 1) and also that both elements are highly correlated in this facies (ST. 3). These "anomalous" concentrations of Pb and Cu in F2 could be caused by variations of extraction efficiency for the different metals in the froth floatation procedure (Ellis et al., 1994). Depending on pulp pH and on other factors, such as the use of ore depressors, recovery of Pb and Cu would be different from other

metals. In practice, the more the use of a "pyrite depressor", the more Pb and Cu would be dumped in tailings (Cook et al., 2020). According to Banos-González and Páez (2013), and Manteca et al. (2014), in "*Lavadero Roberto*" ore processing plant in Portmán Bay pyrite recovery was performed systematically only since 1973, which means more Pb and Cu being dumped into the sea before that date, jointly with substantial amounts of Fe. The later would continue throughout the discharge period, as Fe was not an exploitation target at the time. This may also indicate that the floatation process for pyrite mineral was not effective until 1973, with the above-indicated consequences in terms of Cu and Pb dumping during the first period of sea discharges. The sharp increase of Pb and Cu, but also other elements at the base of F2 (e.g. core GC05; SF. 1A), and the occurrence of pronounced peaks – including those associated with orange layers – (e.g. cores GC52 and GC19; SFs. 1C and 2) might favour this view, though we cannot totally preclude elemental migration down the sedimentary sequence till the F1–F2 contact, at least locally, and subsequent concentrations at specific levels (Sims and Francis, 2010).

5.2. Stratigraphic units and their meaning

The facies described so far (cf. Sections 4 and 5.1) can be organized in stratigraphic units as related to pre-dumping (F1), start of dumping (transitional stage across the study area, F2), dumping period (F3–F6) and post-dumping (F8), the later preceded locally by a transitional stage as well (F7) (Fig. 5). In the paragraphs below we provide elements sustaining such a stratigraphic organization.

The interpretation of F1 as a pre-dumping deposit is supported by the position it consistently occupies in the investigated sequence (i.e. the lowermost one), by the high proportion of shell fragments and vegetal fibres, the highest contents in OC and $CaCO_3$ of all facies, uniform to upwards decreasing trends in physical properties, low values of anthropogenic proxies, and high values of geogenic proxies (Figs. 2 and 4, SFs. 1 to 4, and Table 1). Vegetal fibres mostly correspond to *Posidonia oceanica*, a common sea grass species in the inner continental shelf of Murcia (Ruiz et al., 2015). This species usually forms rather extensive meadows in the Mediterranean Sea, from 5 m depth or less to about 40 m in ideal conditions, which are rooted in sands and coarser sediment they contribute to fix, including abundant shell fragments from organisms living in those meadows. Overall, this results in rather coarse, $CaCO_3$ and OC-rich deposits as those forming F1. Therefore, F1 is interpreted as representing the natural sediments of the continental shelf of Portmán Bay prior to the massive dumping of mine tailings. In stratigraphic terms, F1 is the basal unit of the investigated succession, hereafter named Unit 1 (U1) (Fig. 5A).

F2 appears always atop of F1 and below other facies and seems to be rather widespread according to core data. Physical properties are uniform most often, only with punctual spikes, and roughly similar to those in F1, with the noticeable exception of MS as it reaches much higher values at some intervals (Table 1). Another major difference

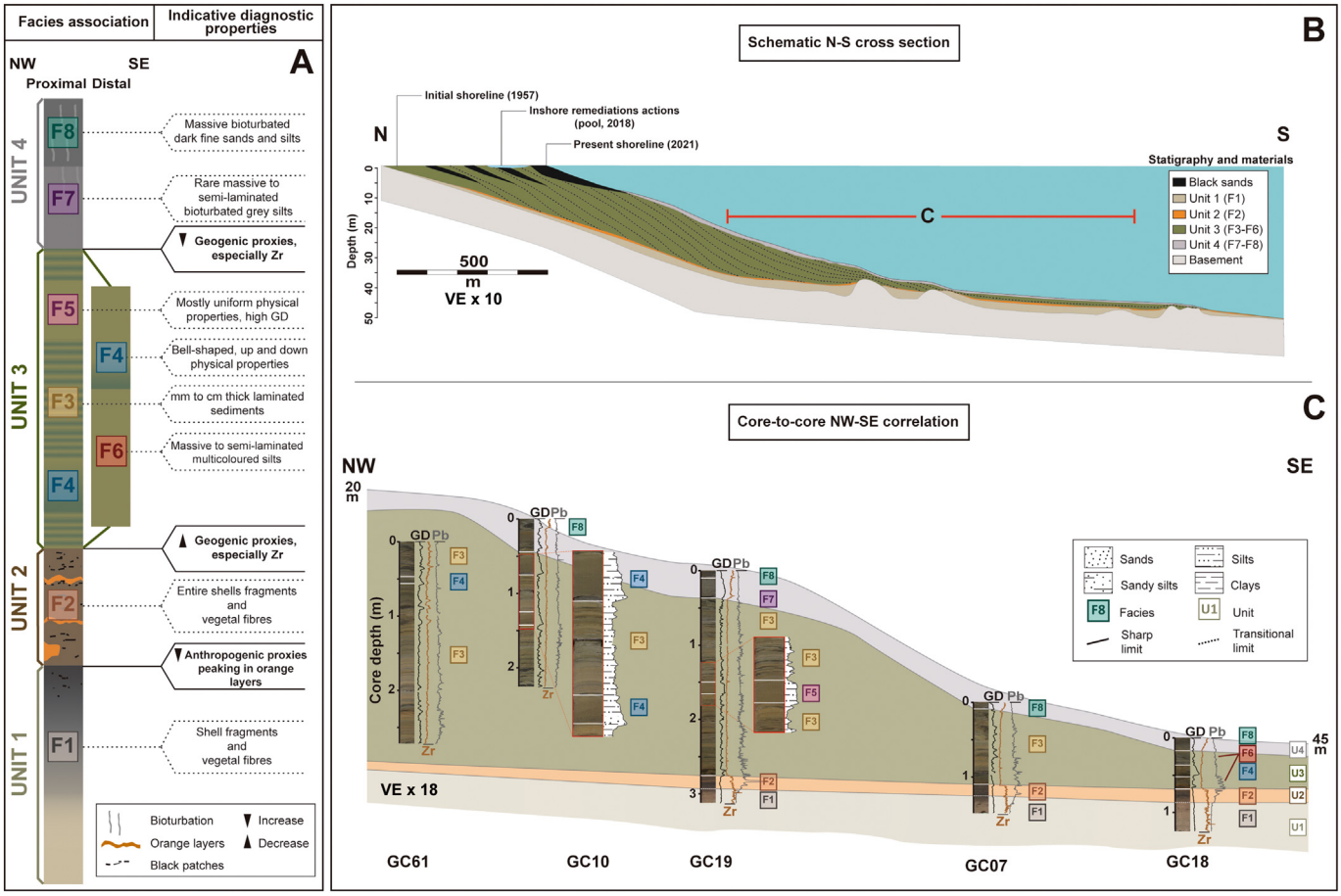

Fig. 5. (A) Facies groupings (proximal to distal) and resulting stratigraphic units in the investigated deposits together with indicative diagnostic properties. **(B)** A general schematic N-S cross section of the area off Portmán Bay covered by the submarine extension of the mine tailings deposit, partly based on Manteca et al. (2014). **(C)** Core-to-core correlation panel along a 1360 m long section across cores GC61, GC10, GC19, GC07 and GC18. Diagnostic properties in facies grouping (A) are purely indicative, and details can be found in the main text and in Table 1. Dotted lines in A represent facies properties, while continuous lines represent unit-scale properties. The red line in B shows the indicative location of the core-to-core correlation in C. Note how U3 rapidly thins seaward (i.e. south-eastern wards) both in B and C. The core-to-core correlation panel in C shows high-resolution colour line scan camera photographs, gamma density (GD; 1.5–2.1 g cm^{-3}), Zr (0–6 cts × 10^3), and Pb (0–600 mg kg^{-1}) logs as representative of physical properties, and of geogenic and anthropogenic proxies. It also includes GD zooms at specific intervals within U3 to show trends. Section C not to scale. For location of sections B and C see Fig. 1.

with respect to F1 is an abrupt increase in anthropogenic proxies, especially Pb and Cu (cf. Section 5.1). Also, there is a relevant decrease in shell fragments and vegetal fibres, a slight reduction of grain size, and a lesser reduction in geogenic proxies, OC and $CaCO_3$ contents. From the mineralogical viewpoint, there are semblances to F1 but also worth noting differences as indicated by the presence of Fe-rich minerals such as siderite and magnetite. All these observations lead to interpreting F2 as formed during the initial stages of mine tailings dumping at sea, in a time period when dumping rates were relatively low (~1000 tons per day; cf. Section 1). F2 actually represents a transitional facies from F1 to the facies above. The very thin nature of F2 or its lack in some cores together with the high metal contents at the very top of F1 is indicative, first, of the locally condensed character of this facies; second, of the still limited arrivals of dumped materials at some core sites at least; and, third, of an initial period, likely of short duration (i.e. a few years) when natural sedimentation and tailings accumulation were contemporaries. All of the above, allow us identifying F2 as a mixed natural and anthropogenic-influenced deposit marking the transition from natural sedimentation conditions to artificially driven ones. From the stratigraphy viewpoint, and from bottom to top, it constitutes Unit 2 (U2) (Fig. 5A).

F3, F4, F5 and F6 appear vertically interstratified in different orders (Figs. 2 and 5, and SFs. 1 to 4) and likely also are horizontally interconnected, as one may evolve to the other, so that they form a facies association. The Zr record, and sometimes the Ca record, allow easily recognizing the boundary between F3 (or another facies in the association) and the underlying F2 (e.g. cores GC05, GC18, GC19; SFs. 1A, 1B, and 2). Also, a more or less pronounced decrease in PW-V values and an increase in MS values correspond to this boundary. An increment in the Zr record marks the upper limit of this facies association.

Considered as a whole, such an association is appreciably heterogeneous at small scale though it might look homogeneous at deposit scale. Obviously, differentiating one from each other instead of considering all of them as a single facies with more or less noticeable internal variability, which would have been the easiest, involves a noticeable effort and a careful analysis of the various log records. On one side, such a grouping is sustained by the obvious affinities partaken by those facies (Table 1), pointing to shared background deposit-forming processes involving hypopycnal flows like those shown by suspensate plumes in Fig. 3 and, mostly, mid-water and near-bottom hyperpycnal flows whereas, on the other side, the recognition of different facies within this package illustrates the internal complexity of the mine tailings submarine deposit off Portmán Bay.

Heterogeneity in F3–F6, and internally in each of the facies, is illustrated by fluctuating patterns and values of physical and chemical properties, including a rather wide range of porosity values (Table 1, and SFs. 1 to 4). This facies association achieves its maximum thickness (>4.20 m in our cores, and probably more as in some cores we did not reach the facies below) the closest to the shoreline discharge pipe and then thins progressively seaward (Fig. 5B and C). Distinguishing between the various facies has been feasible because each of them shows enough differences, especially in terms of physical properties, which suggests somehow distinct bed and in suspension transport and accumulation processes and/or different intensities of them while in action. Differentiating those facies after chemical properties becomes more difficult as, at least for some of them, there is a quite large internal heterogeneity, with high frequency changes succeeding one another (SFs. 1 to 4). In general terms, the geochemical distinctive signal in this facies association is a marked decrease in geogenic elements, especially Zr, even though Ca remains relatively high as amongst the exploited ores there was a quite high proportion of Ca-bearing minerals. It should be kept in mind that whereas ore processing had a homogenisation effect on the tailings finally released to the sea, the exploited ores were themselves heterogeneous and, therefore, different types of "homogenised slurries" were likely dumped, not to talk about possible variations in processing treatments through time. The numerous sedimentary structures in this facies association (Fig. 2) result from both *syn*-sedimentary (e.g. cross-laminations) and post sedimentary processes (e.g. microfracturing and plastic deformation structures), the later likely related to overloading because of very high accumulation rates (cf. Section 5.3), especially in proximal and to a lesser extent intermediate areas. The laminated character of some of those facies eases the visualization of deformation (e.g. F3 but also F4 as shown in Fig. 2), mostly in upper levels.

All physical and chemical evidences clearly points to F3–F6 as deposits formed during the most intense period of tailings discharge, though with variations within that time period and, possibly, also depending on specific locations within the overall area covered by the deposit. Beyond changes in transport and accumulations processes, the development of this set of facies likely relates to fluctuations in discharge, involving rates and materials' character (e.g. grain sizes and composition), and to naturally variable coastal marine dynamics influencing sedimentary processes themselves and tailings dispersal. Occasional cleaning operations of the froth floatation plant might have contributed as well to the observed variability.

From the stratigraphical viewpoint, the F3 to F6 facies association forms a distinct unit that we have named Unit 3 (U3) (Fig. 5A), representing the main period of tailings discharge at sea. Consequently, the upper boundary of U3 tags the end of the mine tailings dumping period in the area.

F8 and the rather infrequent F7 also display noticeable similarities and, therefore, they can be grouped. Physical properties in both facies are more uniform than within those forming U3, showing relatively high values at the bottom and commonly upwards-decreasing trends, likely reflecting re-naturalisation and the installation of more uniform sedimentation conditions across the entire area. Stabilization of MS values around 1000 SI $\times$ 10^{-5} is remarkable, despite some spikes around 3000 SI $\times$ 10^{-5} that correspond to sandy layers, likely magnetite-rich. There are also some bioturbation marks, which support the re-naturalisation view as they indicate some restart of benthic and infaunal activity. The geochemical signature in this cluster shows a gradual increase in geogenic elements, which is especially sharp in the case of Zr, altogether with a gradual decrease or stabilization of anthropogenic elements compared to U3. However, relatively high amounts of As, Zn and Pb, amongst others, still occur in the uppermost centimetres, as also observed by Cerdà-Domènech et al. (2020). The intermediate character of F7 and F8 properties clearly points to a mixture of lag deposits from the top of U3, which seems to be dominant, and strictly post-dumping allochtonous particles from the nearby coastal area. It should be noted that a significant proportion of allochtonous particles result from erosion and subsequent transport of the emerged part of the mine tailings deposit (Fig. 1), thus helping to keep the "tailings heritage" in materials post-dating the dumping period.

Given the above observations, it is clear that these two facies, F7 and F8, represent the end of the mine tailings dumping period and a progressive return to new "natural" conditions that, in any case, are not the same than in the pre-dumping period. Form the stratigraphic viewpoint, these two facies are grouped as Unit 4 (U4) (Fig. 5A), even though it could be discussed if F7 is more transitional in character than F8, and also if F7 could be condensed in some cores, similarly to F2. The rather rare occurrence of F7 in the investigated cores prevents a finer reading and interpretation in this respect.

5.3. Mine tailings sedimentation rates

Since the start and end dates of the dumping of mine tailings at sea are well-known, sedimentation rates along transects or in single points can be easily calculated, provided that the exact depth of the tailings base and top are known to derive the cumulated thickness. In sediment cores, the base of the tailings could be placed at the bottom of U2 representing the transition from pre-dumping to dumping conditions, whereas the top of the tailings should be placed either at the upper

boundary of U3 or at the top of the entire sequence (i.e. at. the seafloor) if we consider that U4 is dominated by lag deposits resulting from reworking of the top of the tailings unit s.str., namely U3.

Our sediment cores reach the bottom of U2 only where the materials above are thin enough (ST. 4). In other words, our cores do not reach the bottom of U2 where the tailings deposit is thicker than the maximum core penetration (i.e. 4.3 m). A simple geometrical projection, similar to the one in Manteca et al. (2014) (Fig. 5B), going from our distal most cores cutting the base of the tailings to the initial shoreline position (Fig. 1), taking also into account the present bathymetry, indicates that the maximum thicknesses of the waste deposit should occur below the modern shoreline or at short distance from it, both in landwards and seawards directions (i.e. in the proximal area of the marine extension of the deposit). It can be inferred that the geometry of the tailings deposit consists of a prograding coastal sedimentary prism that wedges out landwards and seawards from the approximate location of the current shoreline (Fig. 5B). This allows estimating a maximum thickness of about 17–21 m in the most proximal area underwater (<10 m water depth, WD), which is slightly larger than the one that could be derived from the section in Manteca et al. (2014). A similar geometry has been observed in other mine coastal mine tailings deposits extending underwater, such as Black Angel Mine in Greenland and Lihir Mine in Papua New Guinea. In the first, tailings reach about 20 m thick in proximal areas to thin out to less than 20 cm in distal parts. In the Lihir Mine the maximum thickness in proximal parts is over 500 m, from where the tailings deposit thins to a few cm in distal parts, 20 km far from the depocentre (Morello et al., 2016). Beyond the closeness to the main discharge point and the effectiveness of dispersal processes, it is obvious that the topography of the original seafloor may cause local thickenings of tailings deposits in depressions and thinning above former positive relieves, such as the shoreward continuation of the NW–SE oriented rocky ridge to the east of the study area outlined in Fig. 1, or other now buried rocky outcrops. ST. 4, summarizes sedimentation rates of mine tailings obtained from our cores together with those deduced from the geometric estimation of thickness evolution.

As it could be expected, assuming some error margin from inferred geometric reconstructions, sedimentation rates markedly diminish with increasing distance to the tailings main discharge point (DDP) on the shoreline (Fig. 6 and ST. 4), so that rates in excess of half a m y^{-1} in the most proximal area lead to a few tens of cm yr^{-1} in intermediate positions (e.g. ≥12.68 cm yr^{-1} at 24 m depth and 480 m DDP) to barely 0.38 cm yr^{-1} in the most distal part of the deposit's submarine extension, as already suggested by the geometric reconstruction in Manteca et al. (2014) (Fig. 5B).

Sedimentation rates in submarine mine tailing disposal areas are not widely reported in the open literature, nor they cover the full extent from proximal to distal sections. In some cases, they are much lower than the peak values found off Portmán Bay, as illustrated by study cases in Black Angel Mine, Greenland, with sedimentation rates between 0.16 and 1.14 cm yr^{-1} (Elberling et al., 2003) and Repparfjorden in Norway, with rates of 0.07 to 0.43 cm yr^{-1} (Sternal et al., 2017). In the other end is the case of Misima Mine in Papua New Guinea, where sedimentation rates in dumped tailings range from 10 m y^{-1} to 1–2 cm yr^{-1} (Jones and Ellis, 1995). Knowing sedimentation rates in underwater accumulations of mine tailings, especially where they are actually high, is of utmost relevance not only because of suffocation of pre-existing benthic habitats, loading of the water column with suspensates and pollution issues, but also because hypersedimentation may lead to overpressures in the tailings pile subsequently triggering gravitational failures and waste re-sedimentation as described, for instance in STD placements in Fraenfjorden (Burd et al., 2000; Baeten et al., 2020) ND Lillebukt (Bøe et al., 2018).

Peak sedimentation rates in the submarine mine tailings deposit of Portmán Bay are extraordinarily high compared to those in natural coastal environments, including most modern prodeltas, where they are normally in the order of several to a few tens of centimetres per

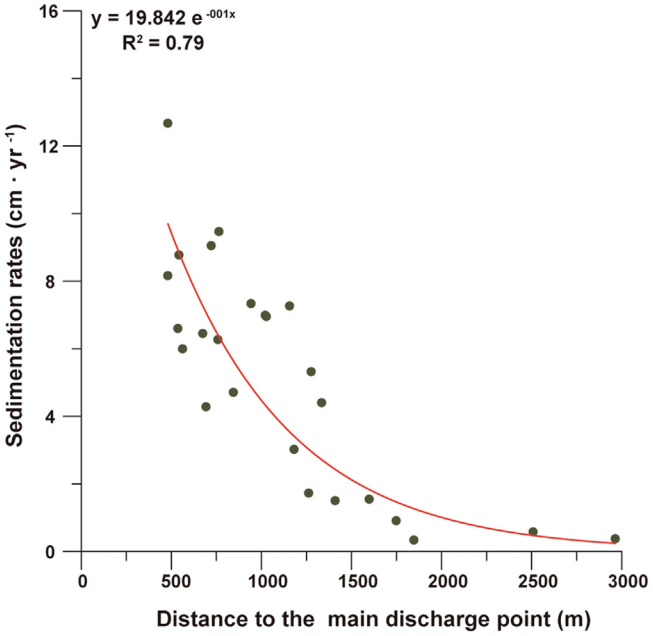

Fig. 6. Evolution of sedimentation rates of mine tailings forming Unit 3 off Portmán Bay as a function of unit thickness in the investigated sediment cores and of core distance to the main discharge point.

year (e.g. Bhattacharya et al., 2020), counting also those off river mouths considered to be high discharge, such as the Yellow River in China (Zhou et al., 2016). As in Portmán Bay, in these natural environments sedimentation rates decrease as a function of distance to the entry point (Fig. 6), as nicely illustrated for instance by a delta lobe that started to develop in 1976 off a new Yellow River mouth, where they range from 5 to 18.6 cm yr^{-1} on the delta front slope to 2 cm yr^{-1} at the prodelta slope toe (Zhou et al., 2016). Only some ultra-high discharge rivers result in sedimentation rates off their mouths that are equivalent —or even higher— than those in areas affected by massive discharges of mine tailings with high sedimentation rates, eventually reaching locations that are far from entry points. For example, sedimentation rates 250 km out of the Amazon River mouth may reach more than 10 cm yr^{-1} (Kuehl et al., 1986, 1996). Also, sedimentation rates of 0.2 cm d^{-1} (or 76 cm yr^{-1} assuming constant sedimentation) have been reported in a submarine canyon fed by Sepik River mouth, in Papua-New Guinea (Walsh and Nittrouer, 2003).

5.4. Burial of Posidonia oceanica meadows

The abundant vegetal fibres and shell fragments in U1 and U2, together with other evidence, as explained above, testify the disappearance by suffocation and burial of *Posidonia oceanica* meadows covering large spans of the seabed in the investigated area prior to the dumping period, as indicated by its systematic presence in all cores containing such units and its forming facies.

Such a benthic community disappearance event took place at the pace of mine tailings spreading from the entry points and of their subsequent accumulation, therefore starting close to shore to gradually advance towards more distal areas. This implies that suffocation and burial progressed as an expanding wave driven by hyperpycnal flows, reaching first the shallower areas and the deeper areas later on. The discharge of tailings into the sea also fed hypopycnal flows, which had the capability to spread to a much wider area than the one reached by hyperpycnal flows (i.e. essentially the one occupied today be the main tailings deposit), subsequently extending the spatial range of disturbance or loss of natural benthic communities, including *P. oceanica*. Actually, the coastal stretch in between Portmán Bay and the city of

Cartagena, to the west, is where *P. oceanica* meadows are dwindling and are less developed along the entire coast of Murcia province (Ruiz et al., 2015). Whereas the release of metals from suspensates into seawater is perfectly illustrated by Bourrin et al. (2021) after a resuspension experiment of the mine tailings in 2014, their harmful effects on organisms was aptly demonstrated after the same experiment by Mestre et al. (2017). Last but not least, the sudden and dramatic shift in environmental conditions resulting from the initiation of massive mine tailings discharge off Portmán Bay must have affected other benthic communities typical of shallow, sediment-starved regions in the western Mediterranean Sea (Canals and Ballesteros, 1997; Cebrián et al., 2000). However, we have not been able to identify evidence for such additional impacts in our sediment cores so far.

While providing a highly relevant number of ecosystem services (Sanchez-Vidal et al., 2021 and references therein), *P. oceanica* communities have been declining in the Mediterranean Sea in terms of areal extent, cover and shoot density at least between 1842 and 2009, according to several authors (Marbà et al., 2014; Telesca et al., 2015). In the Murcia province it has been estimated that about 7.7 km^2 of the meadows have been lost in the last decades, of which 2,75 km^2 would correspond to the area off Portmán Bay because of burial by the mine tailings (Ruiz et al., 2015; Comité de Asesoramiento Científico del Mar Menor, 2017). Beyond burial situations, the occurrence of rather extensive seabed areas now occupied by dead *Posidonia* rhizomes replacing former healthy meadows is quite common in some coastal stretches of the Spanish Mediterranean Sea, such as south of Barcelona city, where signs of recovery have been observed recently (Canals et al., 2020). The causes of the poor state of *P. oceanica* meadows are multiple, including diminution of light penetration because of increased loads and persistence of suspensates and chemical pollution, as it would be the case in the broad area around Portmán dumping site amongst other areas, and also the effects of severe coastal storms (Alcoverro et al., 2020 and references therein).

The impact caused by the 1957 to 1990 massive dumping of mine tailings on the benthic ecosystems of Portmán Bay and the nearby inner continental shelf has thus caused the local extinction of benthic habitats and species for which, 30 years after, there are null signs of recovery. Therefore, a true ecosystem shift has occurred in Portmán Bay and the area nearby because of human activities. Eventually, a comeback of *P. oceanica* to the area sometime in the future seems very unlikely given the resulting dramatic change in the nature of seabed substrate and associated environmental conditions. In case, it would be worth monitoring how benthic habitats in the impacted area evolve through time.

5.5. Man-mediated evolution of Portmán Bay and the nearby inner shelf

Observations and interpretations in previous sections can be summarized in the form of a conceptual model showing how the inner shelf offshore Portmán Bay has evolved through time from initial natural conditions to its current state as a consequence of a long-lasting period of dumping of mine tailings into the area (Fig. 7). This observation-based conceptual model encompasses the last 70 years of Portmán Bay's history.

Prior to the massive dumping period resulting from the shift to large-scale open pit mining operations in the nearby Sierra Minera de Cartagena (cf. Sections 1 and 2.2), environmental conditions within the bay were essentially the natural ones, with typical warm temperate, carbonate-rich sedimentation on a sediment-starved shallow inner shelf including extensive *P. oceanica* meadows that sustained a highly diverse ecosystem, as it could be found in other Mediterranean areas nearby (Canals and Ballesteros, 1997; Cebrián et al., 2000). However, for years before the inception of massive dumping there were already small volume discharges at a few points along the bay's shore by means of a short pipe from "*Lavadero Roberto*" and a natural watercourse that remained dry most of the time, as indicated by the coast-attached plumes in Fig. 3A. This stage is recorded by F1 sediments, identified as stratigraphic U1, and is illustrated by Fig. 7A.

Dumping of mine tailings from 1957 to 1961, with possibly some rather limited amounts in earlier times, triggered the first infill stage of Portmán Bay, led to the development of plumes of suspensates and to the initial spreading of tailings to most of the study area where they started suffocating *P. oceanica* meadows, as observed in our cores, thus leading to the formation of transitional F2 mostly during that period, which corresponds to stratigraphic U2, as shown in Fig. 7B. The regime shift in the marine area nearby Portmán Bay had started. The time of U2 marks an abrupt increment in heavy metal contents in the sediments (Table 1), pointing to the arrival of contaminated particle loads as far as at least 2.5 km from the entry points of mine tailings at the shoreline during this early stage of discharge. The maintenance of similar physical properties of the sediment and rather significant contents of geogenic proxy Zr indicates that the natural signature is partly preserved in F2. Particle transport proceeded mainly through buoyant sediment plumes (i.e. hypopycnal flows) with hyperpycnal flow contributions restricted mostly to the shallowest areas, as indicated by U2 grain size in our cores (i.e. silts lacking of sand grain-sized particles). This was a time when natural benthic habitats, including *P. oceanica* meadows, had to cope with increasing sedimentation rates to survive.

The placement of the first outfall pipe on the cliffs west and out of the Bay in 1961 (cf. Sections 2.2, 4.2 and Figs. 1 and 3) opened the period of massive injection of mine tailings into Portmán Bay and the adjacent marine area. That period lasted till 1990, when dumping ended, i.e. along three decades, and led to the ultimate suffocation and burial of the natural seabed and to the development of a thick mine tailings littoral prism encompassing the different facies (F3–F6) forming stratigraphic U3 (Fig. 7C, D and E). Local accumulation rates peak at more than half a meter per year where U3 is thickest, i.e. close to the modern shoreline, to progressively diminish both landwards and seawards till the tailings prisms wedges out (Figs. 5 and 6, and ST. 4). Such high sedimentation rates, at least locally, and the small-scale deformation structures already observed in our cores (cf. Sections 4.1 and 5.2) point to the likelihood of deformation at larger scales within the mine tailings deposit to accommodate sedimentary overloading, which might result in creepfolds eventually evolving into listric faults where the tailings' pile is thicker. The human-mediated character of U3 is further demonstrated by high values of anthropogenic proxies and overall mineralogy (Table 1). U3 and its building facies resulted from a combination of near-bottom hyperpycnal and hypopycnal flows, likely with a dominance of the first, as shown by the interbedding of intervals with tractive sediment transport structures (F3 and F4) and other intervals that are more homogeneous in character (F5), grain size distributions ranging from unimodal to bimodal and polimodal, or grain size itself with more common occurrence of fine sands than in, for instance, F2. In that respect, it should be kept in mind that peaks in some physical properties such as GD and MS within U3 and more in detail, for example, within F3, correspond to black sandy layers with highly abundant, dense Fe minerals, like magnetite (5.18 g cm^{-3}), pyrite (5 g cm^{-3}), siderite (3.96 g cm^{-3}) or Fe–phyllosilicates and other Fe-oxides (www.mindat.org). Grains of these minerals cannot be transported hypopycnically, as density of standard seawater only is 1.27 g cm^{-3}. Further, tailings deposits in Portmán Bay display GD between 1.5 and 2.2 g cm^{-3}, and more generally 1.7 and 2.2 g cm^{-3} (Table 1). Obviously this does not prevent a fraction of the tailings to be transported by floating through the mediation of buoyancy-facilitating processes (e.g. flocculation, aggregation), but strongly reinforces the prevalence of near-bottom hyperpycnal transport.

We hypothesize that the two straight, positive relief forming rocky ridges outlined in Fig. 1 might have acted as natural barriers preventing a farther spreading of tailings over the seabed. However, this barrier effect was not perfect, as materials belonging to U3 or to transitional F6 above have been identified in cores GC52 (SF. 1C), GC53 and GC27 (Fig. 1), which are all located down flow, to the south and east,

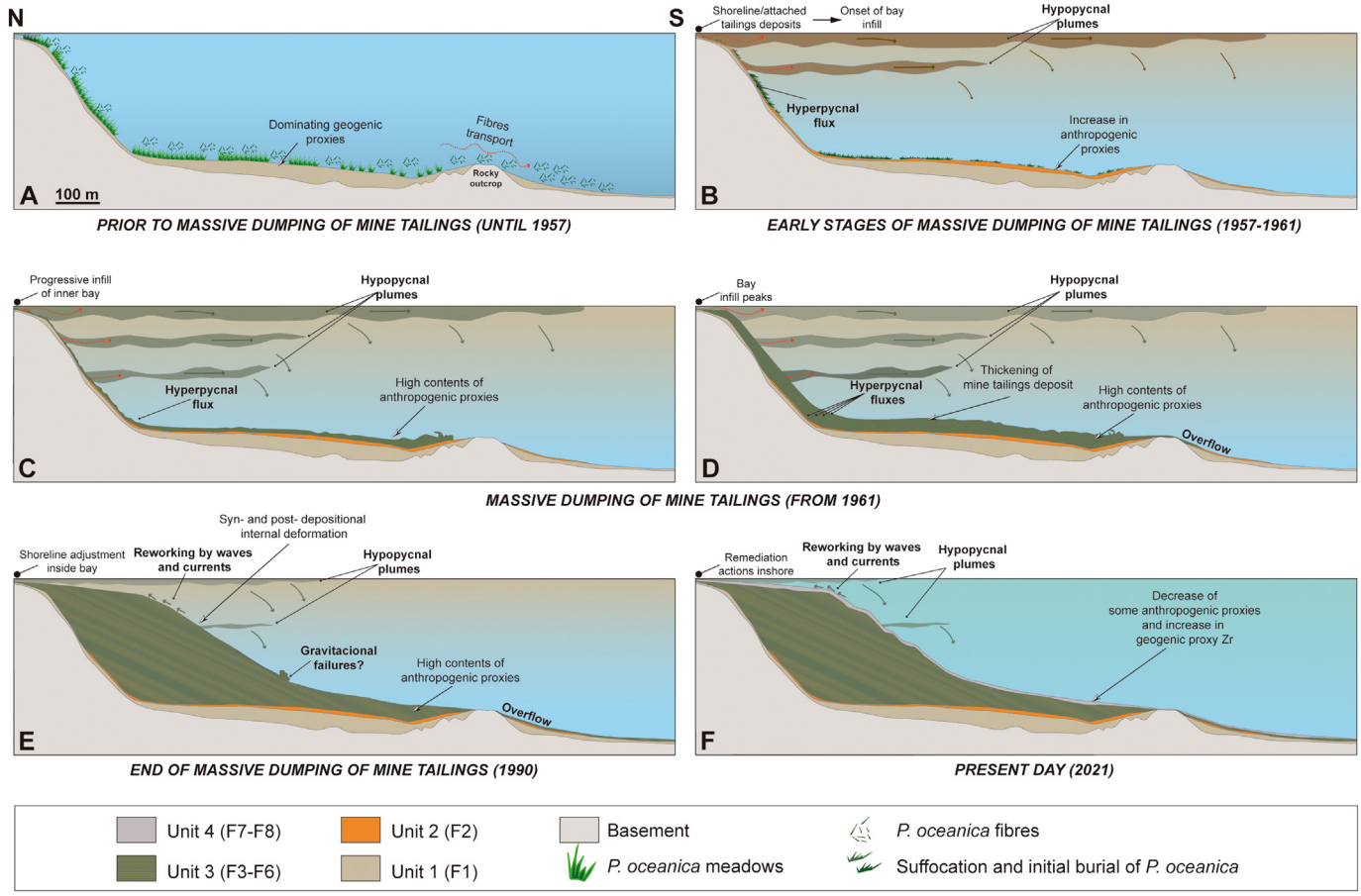

Fig. 7. Conceptual model in a N-S direction (see location in Fig. 1) showing the evolution of inner shelf environments (A, B, C, D, E and F) off Portmán Bay during the last 70 years, including the period prior to massive dumping, and the massive dumping and post-dumping periods. An indicative horizontal scale is provided. Vertical dimension not to scale.

respectively, of those ridges. This is viewed as a clear indication that some overflow occurred, as indicated in Fig. 7D and E, even if restrained. In other words, in Portmán Bay the dispersal of mine tailings dumped at sea was topographically restricted by two main elements, which are the natural shoreline itself and the two parallel NW–SE oriented rocky ridges to the north and south of the main accumulation area, where most of our cores were obtained (Fig. 1). In addition of preventing farther spreading it is also likely that such buttressing of the mine tailings pile forming U3 mitigates further internal deformation at various scales, with the potential to eventually lead to the destabilisation of the deposit. Natural topographic constrictions of various types to mine tailings deposits are rather common occurrence as shown by examples of dumping sites in rivers, lakes, fjords, shallow bays and deep-sea environments, like submarine canyons (e.g. Hay, 1981; Ellis et al., 1995; Berkun, 2005; Bøe et al., 2018).

The post-dumping situation, from 1990 to present times, essentially involves minor sediment contributions from the coastal area, including inputs from rare discharges of local "ramblas", and the reworking by wave action and associated coastal currents of the topmost part of the tailings accumulated during the dumping period (Fig. 7E and F) and of the shoreline. Such a setting can also involve the release of occasional buoyant plumes spreading fine particles to the areas nearby (Fig. 3E and F). This would especially be the case during and after the occurrence of torrential rain and sea storm events (cf. Section 2.1). The consequence is the development of the centimetre thick upper stratigraphic unit U4 made of F7 and F8. This unit marks the reestablishment of bioturbation marks, which were totally lacking in U3 and, therefore, indicates a return tendency towards somehow more "natural" conditions. Varying degrees of recovery back to natural conditions have been identified in other areas affected by massive mine tailings discharge, though not necessarily involving the same species and habitats that were originally present (Kline and Stekoll, 2001; Burd, 2002; Gollner et al., 2017; Trannum et al., 2020).

U4 has a mixed character, including either a transition or sharp shift, depending on each specific location, to deposits holding a residual lag component from underlying materials together with brand new, though limited sedimentary inputs. Hypopycnal flows likely continue playing a role, like possibly rare hyperpycnal flows do. The trend towards more "natural" conditions is reinforced by records of geogenic proxy Zr, which reaches values in F8 that are higher than in underlying U3, and by those from some anthropogenic proxies, such as Pb and Cu, commonly showing lower contents than in most facies forming U3. However, no vegetal fibres neither shell fragments have been found in U4, which indicates that restoring of "true" natural conditions, as the ones recorded in U1, still is far away.

6. Conclusions

A set of 28 sediment gravity cores totalling more than 60 m in length document the history of the transformation of Portmán Bay, in Murcia, SE Spain, from an almost natural state to its current situation, after a 33 years long (1957–1990) intervening period of massive dumping of mine tailings. The comprehensive analysis, mainly by non-destructive, high-resolution geochemical and geophysical techniques, of this set of gravity cores, which were collected over the inner continental shelf extension of the mine tailings deposit, has allowed characterising the sedimentary facies of the materials underlying such deposit, of those constituting the deposit itself, and also of layers formed after the cessation of dumping. Such sedimentary facies have been subsequently grouped in stratigraphic units U1 to U4, of which U1 is pre-dumping,

U2 illustrates the onset of massive dumping and is, therefore, transitional in character, U3 represents the most of the dumping period, and U4 postdates such period and marks a transition towards a new state of sedimentary conditions. Dominant grain sizes in all materials are silts and fine sands, with minor amounts of clays. Sedimentary structures in sediment cores, mainly in facies forming U3, are indicative of sediment transport processes (i.e. hyperpycnal flows) and of *syn*- and post-depositional deformation processes.

Two groups of geochemical proxies have been used to identify geogenic vs. anthropogenic influences on the different facies and units. Zr, Ca, IC and carbonates are good geogenic proxies and as such their contents are higher in pre-dumping materials, i.e. in facies F1 forming U1. Metals occurring in the mined ores, such as Pb, Zn, As, Cu are good anthropogenic proxies. Individual facies F3-F6 forming the main tailings unit U3 have peak Fe contents ranging from 27 to 32%, which are extremely high. MS reflects the presence of Fe-bearing minerals in U3 (100–9300 SI $\times 10^{-5}$) and to a lesser extent in transitional unit U2 (0–6000 SI $\times 10^{-5}$) and in post-dumping U4 (4–3300 SI $\times 10^{-5}$), which is partly made of reworked materials from the top of U3, where the bulk of tailings is. In contrast, the pre-dumping unit U1 shows very low MS (0–150 SI $\times 10^{-5}$). Two anthropogenic proxies, Pb and Cu, peak at transitional unit U2, which marks the onset of tailings disposal in the study area. This could be attributed to scarcely efficient extraction of those metals in the earlier stages of industrial open pit mining and ore processing, though other causes cannot be precluded.

The sedimentation rates of tailings display a pronounced gradient from proximal subareas (i.e. the closest to the main discharge point into the sea), with values eventually in excess of 50 cm yr^{-1} as derived from the geometric reconstruction of the tailings deposit, to the most distal ones, where rates less than 1 cm yr^{-1} have been recorded in our sediment cores. The range of values in these cores, which were obtained in intermediate and distal areas with respect to the location of the main discharge point, is from more than 8 to 12 cm yr^{-1} for cores shallower than 25 m of water depth to less than 0.6 cm yr^{-1} for cores at 53 m depth.

Our core records testify the burial of *P. oceanica* meadows covering the seafloor before the onset of massive mine waste, as evinced by abundant vegetal fibres and carbonate shell fragments in the lowermost unit U1. The characteristics of post-dumping sediments forming U4 are far from those found in pre-dumping sediments, which means that 30 years after the cessation of dumping the original sedimentation (and environmental) conditions in the area have not been restored. Actually, it is very doubtful that they will be reached ever again, at least in a reasonable timeframe.

In our view, challenges ahead and future works to address them should give priority to the following: (i) determining the speciation of metals and metalloids within and around the mine tailings deposit, with the focus on those with the highest toxic potential, so that their bioavailability could be assessed; (ii) deepening the study of the transfer of dissolved elements between the tailings deposit, pore waters and marine waters, and its dispersal patterns and rates in the wider marine environment; (iii) investigating processes of mineral alteration and formation of new minerals within the tailings deposits; and, last but not least, (iv) monitoring the evolution of the habitat from the biological and ecological viewpoints, including all size organisms and compartments.

CRediT authorship contribution statement

Andrea Baza-Varas: Conceptualization, Methodology, Formal analysis, Investigation, Data curation, Visualization, Writing – original draft. **Miquel Canals:** Conceptualization, Funding acquisition, Project administration, Supervision, Writing – review & editing. **Jaime Frigola:** Conceptualization, Methodology, Formal analysis, Investigation, Data curation, Supervision. **Marc Cerdà-Domènech:** Methodology, Formal analysis, Data curation. **Nil Rodés:** Methodology, Formal analysis, Data curation. **Marta Tarrés:** Methodology, Formal analysis. **Anna Sanchez-Vidal:** Conceptualization, Project administration, Methodology, Supervision. **D. Amblàs:** Methodology, Data curation. **X. Rayo:** Methodology, Data curation. **E. Soldevila:** Methodology, Data curation. **J. Rivera:** Methodology, Data curation. **G. Lastras:** Methodology, Data curation. **J. Roqué:** Methodology, Data curation.

Declaration of competing interest

The authors declare that they have no known competing financial interests or personal relationships that could have influenced the work reported in this paper.

Acknowledgements

This research has been carried out as part of NUREIEVA project (ref. CTM2016-75953-C2-1-R) funded by the Spanish Government, and a Catalan Government *Grups de Recerca Consolidats* (excellence research groups) grant to GRC *Geociències Marines* (ref. 2017 SGR 315). A.B.V. acknowledges financial support from APIF PhD fellowship, from University of Barcelona, and J.F. from Serra Húnter Programme of the Generalitat de Catalunya through a tenure-eligible lecturer contract. We would like to thank the crew of R/V *Ángeles Alvariño* and all scientific and technical staff involved in the NUREIEVA-MAR1 research cruise. We thank Montse Guart (Laboratory of Sedimentology from Department of Earth and Ocean Dynamics) and Francisco Menéndez (metal analytical services at CCiTUB) for their assistance with laboratory work. We also thank Pedro Martínez Pagán from the Polytechnical University of Cartagena for providing unreleased aerial photographs.

Appendix A. Supplementary data

Supplementary data to this article can be found online at https://doi.org/10.1016/j.scitotenv.2021.151183.

References

Acosta, J., Fontán, A., Muñoz, A., Muñoz-Martín, A., Rivera, J., Uchupi, E., 2013. The morpho-tectonic setting of the southeast margin of Iberia and the adjacent oceanic algero-Balearic Basin. Mar. Pet. Geol. 45, 17–41. https://doi.org/10.1016/j.marpetgeo.2013.04.005.

Agrawal, Y.C., McCave, I.N., Riley, J.B., 1991. Laser diffraction size analysis. In: Syvitski, J.P.M. (Ed.), Principles, Methods, and Application of Particle Size Analysis. Cambridge University Press, pp. 119–129 https://doi.org/10.1017/CBO9780511626142.012 last consulted in October the 15th.

Alcoverro, T., Marco-Méndez, C., Minguito, M., Boada, J., Prado, P., Sanmartí, N., Muñoz-Ramos, G., Pagés, J.F., Garcia, M., Pérez, M., Seglar, X., Romero, J., 2020. Efectes del temporal Gloria en els ecosistemes de Posidonia oceanica al llarg de la costa catalana. In: Canals, M., Miranda, J. (Eds.), Sobre el temporal Gloria (19-23.01.20), els seus efectes sobre el país i el que se'n deriva. Report de Resposta Ràpida (R3), Institut d'Estudis Catalans, Col·lecció "Informes": Informe de la Secció de Ciències i Tecnologia, Barcelona, pp. 93–101.

Alorda-Kleinglass, A., Garcia-Orellana, J., Rodellas, V., Cerdà-Domènech, M., Tovar-Sánchez, A., Diego-Feliu, M., Trezzi, G., Sánchez-Quilez, D., Sanchez-Vidal, A., Canals, M., 2019. Remobilization of dissolved metals from a coastal mine tailing deposit driven by groundwater discharge and porewater exchange. Sci. Total Environ. 688, 1359–1372. https://doi.org/10.1016/j.scitotenv.2019.06.224.

Auernheimer, C., Chinchon, S., 1997. Calcareous skeletons of sea urchins as indicators of heavy metals pollution. Portman Bay, Spain. Environ. Geol. 29 (1–2), 78–83. https://doi.org/10.1007/s002540050106.

Badawy, W.M., El-Taher, A., Frontasyeva, M.V., Madkour, H.A., Khater, A.E., 2018. Assessment of anthropogenic and geogenic impacts on marine sediments along the coastal areas of egyptian Red Sea. Appl. Radiat. Isot. 140, 314–326. https://doi.org/10.1016/j.apradiso.2018.07.034.

Baeten, N.J., Lepland, A., Bøe, R., Amundsen, A., Chand, S., Longva, O., 2020. Distribution, deposition and impact of submarine mine tailings disposal on the fjord bottom in Frænfjorden, western Norway. Nor. J. Geol. 100 (1). https://doi.org/10.17850/njg100-1-3.

Banning, A., 2021. Geogenic arsenic and uranium in Germany: large-scale distribution control in sediments and groundwater. J. Hazard. Mater. 405, 124–186. https://doi.org/10.1016/j.jhazmat.2020.124186.

Banos-González, I., Páez, P.B., 2013. Portmán: de El Portus Magnus del Mediterráneo occidental a la Bahía Aterrada. Universidad de Murcia. Servicio de Publicaciones 502 p (Editum). ISBN: 978-84-16038-02-2.

Banos-González, I., Páez, P.B., Pérez-Cutillas, P., Selma, M.E., 2017. Análisis de las propuestas de los actores sociales en la recuperación ambiental de la Bahía de Portmán (Región de Murcia). Nuevas perspectivas para un desarrollo sostenible. Cuad. Turismo, 135–154 https://doi.org/10.6018/turismo.40.309641.

Benedicto, J.M., Martínez-Gómez, C., Guerrero, J., Jornet, A., Rodríguez, C., 2008. Metal contamination in Portman Bay (Murcia, SE Spain) 15 years after the cessation of mining activities. Cienc. Mar. 34 (3), 389–398. https://doi.org/10.7773/cm.v34i3.1391.

Berkun, M., 2005. Submarine tailings placement by a copper mine in the deep anoxic zone of the Black Sea. Water Res. 39 (20), 5005–5016. https://doi.org/10.1016/j.watres.2005.10.005.

Bhattacharya, J.P., Howell, C.D., MacEachern, J.A., Walsh, J.P., 2020. Bioturbation, sedimentation rates, and preservation of flood events in deltas. Palaeogeogr. Palaeoclimatol. Palaeoecol. 560, 110049. https://doi.org/10.1016/j.palaeo.2020.110049.

Blott, S.J., Pye, K., 2001. GRADISTAT: a grain size distribution and statistics package for the analysis of unconsolidated sediments. Earth Surf. Process. Landf. 26 (11), 1237–1248. https://doi.org/10.1002/esp.261.

BOE (Boletín Oficial del Estado), 2003. Real Decreto 140/2003, de 7 de febrero, por el que se establecen los criterios sanitarios de la calidad del agua de consumo humano. 45. Ministerio de la Presidencia. available at www.boe.es/buscar/act.php?id=BOE-A-2003-3596 last consulted in October the 15th, 2021.

BOE (Boletín Oficial del Estado), 2011. Resolución de 10 de febrero de 2011, de la Secretaría de Estado de Cambio Climático, por la que se formula declaración de impacto ambiental del proyecto Regeneración y adecuación ambiental de la Bahía de Portmán, término municipal de La Unión, Murcia. 45 (III), 20530-20560. available at www.boe.es/diario_boe/txt.php?id=BOE-A-2011-3494 last consulted in October the 15th, 2021.

Bøe, R., Sandøy, R., Baeten, N.J., Lepland, A., Bellec, V.K., Chand, S., Longva, O., Klug, M., Plassen, L., Schønenberger, J., 2018. Marine mine tailings disposal at Lillebukt, Stjernsundet, North Norway: distribution, sedimentary processes and depositional impacts. Nor. J. Geol. 98 (3). https://doi.org/10.17850/njg98-3-08.

Boës, X., Rydberg, J., Martinez-Cortizas, A., Bindler, R., Renberg, I., 2011. Evaluation of conservative lithogenic elements (Ti, zr, Al, and Rb) to study anthropogenic element enrichments in lake sediments. J. Paleolimnol. 46, 75–87. https://doi.org/10.1007/s10933-011-9515-z.

Bourrin, F., Uusõue, M., Canals, M., Sanchez-Vidal, A., Aubert, D., Menniti, C., Klar, J., 2021. Release of particles and metals into seawater following sediment resuspension of a coastal mine tailings disposal off Portmán Bay, southern Spain. Environ. Sci. Pollut. Res. 1–18. https://doi.org/10.1007/s11356-021-14006-1.

Bridge, J., Demicco, R., 2008. Earth Surface Processes, Landforms and Sediment Deposits. Cambridge University Press https://doi.org/10.1017/CBO9780511805516.

Burd, B.J., 2002. Evaluation of mine tailings effects on a benthic marine infaunal community over 29 years. Mar. Environ. Res. 53 (5), 481–519. https://doi.org/10.1016/S0141-1136(02)00092-2.

Burd, B., Macdonald, R., Boyd, J., 2000. Punctuated recovery of sediments and benthic infauna: a 19-year study of tailings deposition in a British Columbia fjiord. Mar. Environ. Res. 49 (2), 145–175. https://doi.org/10.1016/S0141-1136(99)00058-6.

Busico, G., Cuoco, E., Kazakis, N., Colombani, N., Mastrocicco, M., Tedesco, D., Voudouris, K., 2018. Multivariate statistical analysis to characterize/discriminate between anthropogenic and geogenic trace elements occurrence in the Campania plain, southern Italy. Environ. Pollut. 234, 260–269. https://doi.org/10.1016/j.envpol.2017.11.053.

Canals, M., Ballesteros, E., 1997. Production of carbonate particles by phytobenthic communities on the mallorca-menorca shelf, northwestern Mediterranean Sea. Deep-Sea Res. II Top. Stud. Oceanogr. 44 (3–4), 611–629. https://doi.org/10.1016/S0967-0645(96)00095-1.

Canals, M., Ballesteros, E., Amblàs, D., Jordana, E., Pinedo, S., 2020. Cartografia dels fons marins de Sitges: batimetria, sedimentologia i hàbitats bentònics. GRC Geociències Marines, Universitat de Barcelona, i Centre d'Estudis Avançats de Blanes, Consejo Superior de Investigaciones Científicas. Informe, Ajuntament de Sitges 94 + annexos.

Cebrián, E., Ballesteros, E., Canals, M., 2000. Shallow rocky bottom benthic assemblages as calcium carbonate producers in the Alboran Sea (southwestern Mediterranean). Oceanol. Acta 23 (3), 311–322. https://doi.org/10.1016/S0399-1784(00)00131-6.

Cerdà-Domènech, M., Frigola, J., Sanchez-Vidal, A., Canals, M., 2020. Calibrating high resolution XRF core scanner data to obtain absolute metal concentrations in highly polluted marine deposits after two case studies off Portmán Bay and Barcelona, Spain. Sci. Total Environ. 717, 134778. https://doi.org/10.1016/j.scitotenv.2019.134778.

Comité de Asesoramiento Científico del Mar Menor, 2017. Análisis de soluciones para el objetivo del vertido cero al Mar Menor proveniente del Campo de Cartagena. Apéndice 18: Consejería de Agua, Agricultura y Medio Ambiente, Región de Murcia, pp. 294–315.

Conesa, H.M., Schulin, R., Nowack, B., 2008. Mining landscape: a cultural tourist opportunity or an environmental problem?: the study case of the Cartagena-La Unión Mining District (SE Spain). Ecol. Econ. 64 (4), 690–700. https://doi.org/10.1016/j.ecolecon.2007.06.023.

Cook, R., Monyake, K.C., Hayat, M.B., Kumar, A., Alagha, L., 2020. Prediction of flotation efficiency of metal sulfides using an original hybrid machine learning model. Eng. Rep. 2 (6), 12167. https://doi.org/10.1002/eng2.12167.

Debret, M., Sebag, D., Desmet, M., Balsam, W., Copard, Y., Mourier, B., Susperrigui, A.-S., Arnaud, F., Bentaleb, I., Chapron, E., Lallier-Vergès, E., Winiarski, T., 2011. Spectrocolorimetric interpretation of sedimentary dynamics: the new "Q7/4 diagram". Earth Sci. Rev. 109 (1–2), 1–19. https://doi.org/10.1016/j.earscirev.2011.07.002.

Delshab, H., Farshchi, P., Keshavarzi, B., 2017. Geochemical distribution, fractionation and contamination assessment of heavy metals in marine sediments of the Asaluyeh port, Persian Gulf. Mar. Pollut. Bull. 115 (1–2), 401–411. https://doi.org/10.1016/j.marpolbul.2016.11.033.

Dold, B., 2014. Submarine tailings disposal (STD) — a review. Minerals 4 (3), 642–666. https://doi.org/10.3390/min4030642.

Dou, Y., Li, J., Zhao, J., Hu, B., Yang, S., 2013. Distribution, enrichment and source of heavy metals in surface sediments of the eastern Beibu Bay, South China Sea. Mar. Pollut. Bull. 67 (1–2), 137–145. https://doi.org/10.1016/j.marpolbul.2012.11.022.

Duodu, G.O., Goonetilleke, A., Ayoko, G.A., 2017. Potential bioavailability assessment, source apportionment and ecological risk of heavy metals in the sediment of Brisbane River estuary, Australia. Mar. Pollut. Bull. 117 (1–2), 523–531. https://doi.org/10.1016/j.marpolbul.2017.02.017.

Durán, R., Guillén, J., Rivera, J., Lobo, F.J., Muñoz, A., Fernández-Salas, L.M., Acosta, J., 2018. Formation, evolution and present-day activity of offshore sand ridges on a narrow, tideless continental shelf with limited sediment supply. Mar. Geol. 397, 93–107. https://doi.org/10.1016/j.margeo.2017.11.001.

Elberling, B., Knudsen, K.L., Kristensen, P.H., Asmund, G., 2003. Applying foraminiferal stratigraphy as a biomarker for heavy metal contamination and mining impact in a fiord in West Greenland. Mar. Environ. Res. 55 (3), 235–256. https://doi.org/10.1016/s0141-1136(02)00219-2.

Ellis, D., Poling, G., Pelletier, C., 1994. Case studies of submarine tailings disposal: volume II – worldwide case histories and screening criteria. U.S. Bureau Mines Open File Rep. 37 (94) 136 p.

Ellis, D.V., Pedersen, T.F., Poling, G.W., Pelletier, C., Horne, I., 1995. Review of 23 years of STD: island copper mine. Canada. Marine Georesources and Geotechnology 13 (1–2), 59–99. https://doi.org/10.1080/10641199509388279.

Fernández-Salas, L.M., Durán, R., Mendes, I., Galparsoro, I., Lobo, F.J., Bárcenas, P., Rosa, F., Ribó, M., García-Gil, S., Carrara, G., Roque, C., Canals, M., 2015. Shelves of the Iberian Peninsula and the Balearic Islands (I): morphology and sediment types. Bol. Geol. Min. 126 (2–3), 327–376.

Frigola, J., Canals, M., Mata, P., 2015. Techniques for the non-destructive and continuous analysis of sediment cores. Application in the iberian continental margin. Bol. Geol. Min. 126 (2–3), 609–634.

Gambi, C., Dell'Anno, A., Corinaldesi, C., Martire, M.L., Musco, L., Da Ros, Z., Armiento, G., Danovaro, R., 2020. Impact of historical contamination on meiofaunal assemblages: the case study of the bagnoli-Coroglio Bay (southern Tyrrhenian Sea). Mar. Environ. Res. 156, 104907. https://doi.org/10.1016/j.marenvres.2020.104907.

García-García, C., 2004. Impacto y riesgo medioambiental en los residuos minerometalúrgicos de la Sierra de Cartagena-La Unión. PhD ThesisUniversidad Politécnica de Cartagena, Cartagena, Spain 388 p. + ann.

García-Lorenzo, M.L., Pérez-Sirvent, C., Martínez-Sánchez, M.J., Molina-Ruiz, J., 2012. Trace elements contamination in an abandoned mining site in a semiarid zone. J. Geochem. Explor. 113, 23–35. https://doi.org/10.1016/j.gexplo.2011.07.001.

García-Lorenzo, M.L., Martínez-Sánchez, M.J., Pérez-Sirvent, C., Agudo, I., Recio, C., 2014a. Isotope geochemistry of waters affected by mining activities in sierra minera and Portman Bay (SE, Spain). Appl. Geochem. 51, 139–147. https://doi.org/10.1016/j.apgeochem.2014.10.002.

García-Lorenzo, M.L., Pérez-Sirvent, C., Molina-Ruiz, J., Martínez-Sánchez, M.J., 2014b. Mobility indices for the assessment of metal contamination in soils affected by old mining activities. J. Geochem. Explor. 147, 117–129. https://doi.org/10.1016/j.gexplo.2014.06.012.

Gollner, S., Kaiser, S., Menzel, L., Jones, D.O., Brown, A., Mestre, N.C., van Oevelen, D., Menot, L., Colaço, A., Canals, M., Cuvelier, D., Durden, J.M., Gebrik, A., Egho, G.A., Haeckel, M., Marcon, Y., Mevenkamp, L., Morato, T., Pham, C.K., Purser, A., Sànchez-Vidal, A., Vanreusel, A., Vink, A., Arbizu, P.M., 2017. Resilience of benthic deep-sea fauna to mining activities. Mar. Environ. Res. 129, 76–101. https://doi.org/10.1016/j.marenvres.2017.04.010.

Gómez-Garcia, C., Martin-Hernández, F., García, J.A.L., Martínez-Pagan, P., Manteca, J.I., Carmona, C., 2015. Rock magnetic characterization of the mine tailings in Portman Bay (Murcia, Spain) and its contribution to the understanding of the bay infilling process. J. Appl. Geophys. 120, 48–59. https://doi.org/10.1016/j.jappgeo.2015.06.008.

Gunn, D., Best, A., 1998. A new automated nondestructive system for high resolution multi-sensor core logging of open sediment cores. Geo-Mar. Lett. 18, 70–77. https://doi.org/10.1007/s003670050054.

Hay, A.E., 1981. Submarine Channel Formation and Acoustic Remote Sensing of Suspended Sediments and Turbidity Currents in Rupert Inlet, BC. Doctoral dissertationUniversity of British Columbia, Canada 326 p.

Hayashi, K.I., Fujisawa, H., Holland, H.D., Ohmoto, H., 1997. Geochemistry of ~1.9 Ga sedimentary rocks from northeastern Labrador, Canada. Geochim. Cosmochim. Acta 61 (19), 4115–4137. https://doi.org/10.1016/S0016-7037(97)00214-7.

IMO (International Maritime Organization), 1972. The London Convention. Convention on the prevention of marine pollution by dumping wastes and other matter. available at www.imo.org/en/OurWork/Environment/Pages/London-Convention-Protocol.aspx last consulted in October the 15th, 2021.

Jones, S.G., Ellis, D.V., 1995. Deep water STD at the misima gold and silver mine, Papua, New Guinea. Mar. Georesour. Geotechnol. 13, 183–200. https://doi.org/10.1016/0148-9062(96)82026-2.

Kabir, S.Z., Rabbi, F., Chowdhury, M.B., Akbar, D., 2015. A review of mine closure planning and practice in Canada and Australia. World Rev. Bus. Res. 5 (3), 140–159.

Kawatra, S.K., 2011. Fundamental principles of froth flotation. In: Darling, P. (Ed.), SME Mining Engineering Handbook. Society for Mining, Metallurgy, and Exploration, Englewood (CO), USA, pp. 1517–1532.

Kline, E.R., Stekoll, M.S., 2001. Colonization of mine tailings by marine invertebrates. Mar. Environ. Res. 51 (4), 301–325. https://doi.org/10.1016/S0141-1136(00)00105-7.

Koinig, K.A., Shotyk, W., Lotter, A.F., Ohlendorf, C., Sturm, M., 2003. 9000 years of geochemical evolution of lithogenic major and trace elements in the sediment of an alpine lake - the role of climate, vegetation, and land-use history. J. Paleolimnol. 30, 307–320. https://doi.org/10.1023/A:1026080712312.

Koski, R.A., 2012. Metal dispersion resulting from mining activities in coastal environments: a pathways approach. Oceanography 25 (2), 170–183. https://doi.org/10.5670/oceanog.2012.53.

Kuehl, S.A., Demaster, D.J., Nittrouer, C.A., 1986. Nature of sediment accumulation on the Amazon continental shelf. Cont. Shelf Res. 6, 209–225. https://doi.org/10.1016/0278-4343(86)90061-0.

Kuehl, S.A., Nittrouer, C.A., Allison, M.A., Faria, L.E.C., Dukat, D.A., Jaeger, J.M., Pacioni, T.D., Figueiredo, A.G., Underkoffler, E.C., 1996. Sediment deposition, accumulation, and seabed dynamics in an energetic fine-grained coastal environment. Cont. Shelf Res. 16, 787–815. https://doi.org/10.1016/0278-4343(95)00047-x.

Last, W.M., Smol, J.P., 2002. An introduction to basin analysis, coring, and chronological techniques used in Paleolimnology. In: Last, W.M., Smol, J.P. (Eds.), Tracking Environmental Change Using Lake Sediments. Developments in Paleoenvironmental Research. vol 1. Springer, Dordrecht. https://doi.org/10.1007/0-306-47669-X_1.

Llull, R.M., Garí, M., Canals, M., Rey-Maquieira, T., Grimalt, J.O., 2017. Mercury concentrations in lean fish from the Western Mediterranean Sea: dietary exposure and risk assessment in the population of the Balearic Islands. Environ. Res. 158, 16–23. https://doi.org/10.1016/j.envres.2017.05.033.

Maldonado, A., Zamarreño, I., 1983. Modelos sedimentarios en las plataformas continentales del Mediterráneo español: factores de control, facies y procesos que rigen su desarrollo. Estudio oceanográfico de la Plataforma Continental. Proyecto de Investigacion Cooperatiava Hispano-Norteamericana, Madrid, pp. 24–83.

Manteca, J.I., Ovejero, G., 1992. Los yacimientos Zn. Pb, Ag-Fe del distrito minero de La Unión. Recursos Minerales de España. CSIC, Madrid, pp. 1085–1102.

Manteca, J.I., López García, J.Á., Oyarzun, R., Carmona, C., 2014. The beach placer iron deposit of Portman Bay, Murcia, SE Spain: the result of 33 years of tailings disposal (1957–1990) to the Mediterranean seaside. Mineral. Deposita 49, 777–783. https://doi.org/10.1007/s00126-014-0511-x.

Marbà, N., Díaz-Almela, E., Duarte, C.M., 2014. Mediterranean seagrass (Posidonia oceanica) loss between 1842 and 2009. Biol. Conserv. 176, 183–190. https://doi.org/10.1016/j.biocon.2014.05.024.

Martínez-Gómez, C., Fernández, B., Benedicto, J., Valdés, J., Campillo, J.A., León, V.M., Vethaak, A.D., 2012. Health status of red mullets from polluted areas of the spanish Mediterranean coast, with special reference to Portmán (SE Spain). Mar. Environ. Res. 77, 50–59. https://doi.org/10.1016/j.marenvres.2012.02.002.

Martínez-Sánchez, M.J., Navarro, M.C., Pérez-Sirvent, C., Marimón, J., Vidal, J., García-Lorenzo, M.L., Bech, J., 2008. Assessment of the mobility of metals in a mining-impacted coastal area (Spain, Western Mediterranean). J. Geochem. Explor. 96 (2–3), 171–182. https://doi.org/10.1016/j.gexplo.2007.04.006.

Martínez-Sánchez, M.J., Martínez-López, S., García-Lorenzo, M.L., Martínez-Martínez, L.B., Pérez-Sirvent, C., 2011. Evaluation of arsenic in soils and plant uptake using various chemical extraction methods in soils affected by old mining activities. Geoderma 160 (3–4), 535–541. https://doi.org/10.1016/j.geoderma.2010.11.001.

Matínez-Sánchez, M.J., Pérez-Sirvent, C., García-Lorenzo, M.L., Martínez, S., de Baño, J.M.V., Gonzalez, E., Perez, V., Martínez, L.B., Hernandez, C., 2013. Las arenas de la Bahía de portman: ¿residuo o mena de hierro? Macla Rev. Soc. Esp. Mineral. 17, 69–70.

Martínez-Sánchez, M.J., García-Lorenzo, M.L., Martínez-López, S., Martínez-Martínez, L.B., Pérez-Hernández, C., Pérez-Sirvent, C., 2015. El análisis de riesgos Para la salud humana, en el paradigma de la gestión de suelos contaminados: el Caso de la Bahía de Portmán. Rev. Salud Ambient. 15 (2), 103–112.

Mateos, J.C.R., 2001. The case of the aznalcollar mine and its impacts on coastal activities in southern Spain. Ocean Coast. Manag. 44 (1–2), 105–118. https://doi.org/10.1016/S0964-5691(00)00081-8.

Mestre, N.C., Rocha, T.L., Canals, M., Cardoso, C., Danovaro, R., Dell'Anno, A., Gambi, C., Regoli, F., Sànchez-Vidal, A., Bebianno, M.J., 2017. Environmental hazard assessment of a marine mine tailings deposit site and potential implications for deep-sea mining. Environ. Pollut. 228, 169–178. https://doi.org/10.1016/j.envpol.2017.05.027.

Millot, C., Taupier-Letage, I., 2005. Circulation in the Mediterranean Sea. In: Saliot, A. (Ed.), The Mediterranean Sea. Handbook of Environmental Chemistry. vol 5. Springer, Berlin, Heidelberg. https://doi.org/10.1007/b107143.

MINEMET, 1974. Peñarroya-España minerals Pb-Zn de la mine de Roberto (Carthagène). Tentatives d'amélioration des résultas de la flotation. Centre d'études et d'analyses des minerais et métaux, Internal Report.

Monjezi, M., Shahriar, K., Dehghani, H., Namin, F.S., 2009. Environmental impact assessment of open pit mining in Iran. Environ. Geol. 58 (1), 205–216. https://doi.org/10.1007/s00254-008-1509-4.

Morello, E.B., Haywood, M.D., Brewer, D.T., Apte, S.C., Asmund, G., Kwong, Y.J., Dennis, D., 2016. The ecological impacts of submarine tailings placement. Oceanogr. Mar. Biol. 54, 315–366. https://doi.org/10.1201/9781315368597-7.

Morrison-Saunders, A., McHenry, M.P., Rita Sequeira, A., Gorey, P., Mtegha, H., Doepel, D., 2016. Integrating mine closure planning with environmental impact assessment: challenges and opportunities drawn from african and australian practice. Impact Assess. Proj. Apprais. 34 (2), 117–128. https://doi.org/10.1080/14615517.2016.1176407.

Natali, C., Bianchini, G., 2018. Natural vs anthropogenic components in sediments from the Po River delta coastal lagoons (NE Italy). Environ. Sci. Pollut. Res. 25, 2981–2991. https://doi.org/10.1007/s11356-017-0986-y.

Noble, B.F., Bronson, J.E., 2005. Integrating human health into environmental impact assessment: case studies of Canada's northern mining resource sector. Arctic 58 (4), 395–405. https://doi.org/10.14430/arctic453.

Odhiambo, B.K., Macdonald, R.W., O'Brien, M.C., Harper, J.R., Yunker, M.B., 1996. Transport and fate of mine tailings in a coastal fjord of British Columbia as inferred from the sediment record. Sci. Total Environ. 191 (1–2), 77–94. https://doi.org/10.1016/0048-9697(96)05250-3.

Oen, I.S., Fernández, J.C., Manteca, J.I., 1975. The lead-zinc and associated ores of La Unión, Sierra de Cartagena, Spain. Econ. Geol. 70 (7), 1259–1278. https://doi.org/10.2113/gsecongeo.70.7.1259.

OJEC (Official Journal of the European Communities), 1998. Council Directive 98/83/EC of 3 November 1998 on the quality of water intended for human consumption. L330, 32-54. Doctoral dissertation https://eur-lex.europa.eu/legal-content/ES/TXT/?uri=celex%3A31998L0083 326 p.

OJEU (Official Journal of the European Union), 2009. Decision of 30 April 2009 completing the technical requirements for waste characterization laid down by Directive 2006/21/EC of the European Parliament and of the Council on the management of waste from extractive industries. L110, 48-51. https://eur-lex.europa.eu/legal-content/EN/TXT/?uri=celex:32009D0360 110 p.

Oyarzun, R., Higueras, P., Lillo, J., 2011. Minería ambiental: una introducción a los impactos y su remediación. Ediciones GEMM - Aula2puntonet. https://doi.org/10.13140/2.1.4341.5686 337 p.

Oyarzun, R., Manteca Martínez, J.I., López García, J.A., Carmona, C., 2013. An account of the events that led to full bay infilling with sulfide tailings at portman (Spain), and the search for "black swans" in a potential land reclamation scenario. Sci. Total Environ. 454 (455), 245–249. https://doi.org/10.1016/j.scitotenv.2013.03.030.

Pauc, H., Thibault, M., 1976. L'hydrodynamique et la dynamique des matériaux en suspension en baie de Portman (Province de Murcie, Espagne). Bull. BRGM IV (3), 211–221 (12th series).

Peña, J.A., Manteca, J.I., Martínez-Pagán, P., Teixidó, T., 2013. Magnetic gradient map of the mine tailings in Portman Bay (Murcia, Spain) and its contribution to the understanding of the bay infilling process. J. Appl. Geophys. 95, 115–120. https://doi.org/10.1016/j.jappgeo.2013.05.011.

Ramirez-Llodra, E., Trannum, H.C., Evenset, A., Levin, L.A., Andersson, M., Finne, T.E., Hilario, A., Flem, B., Christensen, G., Schaanning, M., Vanreusel, A., 2015. Submarine and deep-sea mine tailing placements: a review of current practices, environmental issues, natural analogs and knowledge gaps in Norway and internationally. Mar. Pollut. Bull. 97 (1–2), 13–35. https://doi.org/10.1016/j.marpolbul.2015.05.062.

Richter, T.O., Van der Gaast, S., Koster, B., Vaars, A., Gieles, R., de Stigter, H.C., de Haas, H., van Weering, T.C., 2006. The avaatech XRF Core scanner: technical description and applications to NE Atlantic sediments. Geol. Soc. Lond., Spec. Publ. 267 (1), 39–50. https://doi.org/10.1144/GSL.SP.2006.267.01.03.

Robles-Arenas, V.M., 2007. Caracterización hidrogeológica de la Sierra de Cartagena-La Unión (SE de la Península Ibérica. Impacto de la minería abandonada sobre el medio hídrico. Universidad Politécnica de Cataluña. available at https://upcommons.upc.edu/handle/2117/93557 last consulted in October the 15th, 2021.

Robles-Arenas, V.M., Rodríguez, R., García, C., Manteca, J.I., Candela, L., 2006. Sulphide-mining impacts in the physical environment: sierra de Cartagena-La Unión (SE Spain) case study. Environ. Geol. 51, 47–64. https://doi.org/10.1007/s00254-006-0303-4.

Roche, C., Thygesen, K., Baker, E., 2017. Mine tailings storage: safety is no accident. A UNEP Rapid Response Assessment. Nairobi and Arendal: United Nations Environment Programme and GRID-Arendal. 31 (05), 70 p.

Ross, P.S., Bourke, A., 2017. High-resolution gamma ray attenuation density measurements on mining exploration drill cores, including cut cores. J. Appl. Geophys. 136, 262–268. https://doi.org/10.1016/j.jappgeo.2016.11.012.

Rothwell, R.G., Rack, F.R., 2006. New techniques in sediment core analysis: an introduction. Geol. Soc. Lond., Spec. Publ. 267 (1), 1–29. https://doi.org/10.1144/GSL.SP.2006.267.01.01.

Ruiz, J.M., Romero, J., 2001. Effects of in situ experimental shading on the Mediterranean seagrass Posidonia oceanica. Mar. Ecol. Prog. Ser. 215, 107–120. https://doi.org/10.3354/meps215107.

Ruiz, J.M., Guillén, J.E., Ramos Segura, A., Otero, M., 2015. Atlas de las praderas marinas de España. IEO/IEL/UICN, Murcia-Alicante-Málaga, p. 681.

Sabaté, A.A., Melgarejo, J.C., Tauler, E., Torró, L., Manteca, J.I., Arnold, M., 2015. Ore deposits in La Unión-Portmán District: mineralogical and geochemical characterization. Proceedings of the 13th SGA Biennal Meeting-Nancy, France, pp. 355–358.

Sanchez-Vidal, A., Canals, M., de Haan, W.P., Romero, J., Veny, M., 2021. Seagrasses provide a novel ecosystem service by trapping marine plastics. Sci. Rep. 11, 254. https://doi.org/10.1038/s41598-020-79370-3.

Sims, D.B., Francis, A., 2010. Anthropogenic influences on geogenic trace elements and contamination in wash sediments from historical mining activities in the carnation wash system, Nelson, Nevada (USA). Int. J. Soil Sed. Water 3 (1), 2.

Sindern, S., Tremöhlen, M., Dsikowitzky, L., Gronen, L., Schwarzbauer, J., Siregar, T.H., Ariyani, F., Irianto, H.E., 2016. Heavy metals in river and coast sediments of the Jakarta Bay region (Indonesia) - geogenic versus anthropogenic sources. Mar. Pollut. Bull. 110 (2), 624–633. https://doi.org/10.1016/j.marpolbul.2016.06.003.

SMMPE, S.A. (Sociedad Minero Metalúrgica de Peñarroya-España, S.A.), 1970. Las explotaciones de plomo y cinc en la Sierra de Cartagena (folleto divulgativo) 82 p.

SMMPE, S.A. (Sociedad Minero Metalúrgica de Peñarroya-España, S.A.), 1980. Lavadero Roberto. Monografía 1980 (documento interno) 85 p.

SMMPE, S.A. (Sociedad Minero Metalúrgica de Peñarroya-España, S.A.), 1984. Libro del Centenario. 1881-1981. Sociedad Minera y Metalúrgica de Peñarroya-España SA, Cartagena.

SMMPE, S.A. (Sociedad Minero Metalúrgica de Peñarroya-España, S.A.), 1985. Centro minero de la Sociedad Minera y Metalúrgica de Peñarroya-España, S.A. en Cartagena-La Unión (folleto divulgativo) 23 p.

Sternal, B., Junttila, J., Skirbekk, K., Forwick, M., Carroll, J., Pedersen, K.B., 2017. The impact of submarine copper mine tailing disposal from the 1970s on repparfjorden, northern Norway. Mar. Pollut. Bull. 120 (1–2), 136–153. https://doi.org/10.1016/j.marpolbul.2017.04.054.

Telesca, L., Belluscio, A., Criscoli, A., Ardizzone, G., Apostolaki, E.T., Fraschetti, S., Gristina, M., Knittweis, L., Martin, C.S., Pergent, G., Alagna, A., Badalamenti, F., Garofalo, G.,

Gerakaris, V., Pace, M.L., Pergent-Martini, C., Salomidi, M., 2015. Seagrass meadows (Posidonia oceanica) distribution and trajectories of change. Sci. Rep. 5 (1), 1–14. https://doi.org/10.1038/srep12505.

Trannum, H.C., Næss, R., Gundersen, H., 2020. Macrofaunal colonization of mine tailings impacted sediments. Sci. Total Environ. 708, 134866. https://doi.org/10.1016/j.scitotenv.2019.134866.

Tjallingii, R., Röhl, U., Kölling, M., Bickert, T., 2007. Influence of the water content on X-ray fluorescence core-scanning measurements in soft marine sediments. Geochem. Geophys. Geosyst. 8 (2). https://doi.org/10.1029/2006GC001393.

Twardowska, I., Kyziol, J., 2003. Sorption of metals onto natural organic matter as a function of complexation and adsorbent-adsorbate contact mode. Environ. Int. 28 (8), 783–791. https://doi.org/10.1016/S0160-4120(02)00106-X.

UNEP (United Nations Enivonment Programme), 1995. The convention for the protection of the Mediterranean Sea against pollution and related protocols. available at https://www.unep.org/unepmap/who-we-are/barcelona-convention-and-protocols last consulted in October the 15th, 2021.

Vilar, J.B., Bruno, P.M.E., Gutiérrez, J.C.F., 1991. La minería murciana contemporánea (1930-1985). EDITUM 256 p.

Vare, L.L., Baker, M.C., Howe, J.A., Levin, L.A., Neira, C., Ramirez-Llodra, E.Z., Reichelt-Brushett, A., Rowden, A.A., Shimmield, T.M., Simpson, S.L., Soto, E.H., 2018. Scientific considerations for the assessment and management of mine tailings disposal in the deep sea. Front. Mar. Sci. 5, 17. https://doi.org/10.3389/fmars.2018.00017.

Vogt, C., 2013. International assessment of marine and riverine disposal of mine tailings. Final Report Adopted by the International Maritime Organization, London Convention/Protocol. available at www.CraigVogt.com last consulted in October the 15th, 2021.

Walder, I., 2014. Sub-sea Tailings Deposition Evaluation Guideline, prEN/TR-9432. Technical Report. 2 110 p.

Walsh, J.P., Nittrouer, C.A., 2003. Contrasting styles of off-shelf sediment accumulation in New Guinea. Mar. Geol. 196 (3–4), 105–125. https://doi.org/10.1016/s0025-3227(03)00069-0.

Warren, L.A., Haack, E.A., 2001. Biogeochemical controls on metal behavior in freshwater environments. Earth Sci. Rev. 54 (4), 261–320. https://doi.org/10.1016/S0012-8252(01)00032-0.

Zhou, L., Liu, J., Saito, Y., Gao, M., Diao, S., Qiu, J., Pei, S., 2016. Modern sediment characteristics and accumulation rates from the delta front to prodelta of the Yellow River (Huanghe). Geo-Mar. Lett. 36 (4), 247–258. https://doi.org/10.1007/s00367-016-0442-x.

www.mindat.org, 2021. The World's Largest Open Database of Minerals, Rocks, Meteorites and the Localities They Come From last consulted in October the 15th.